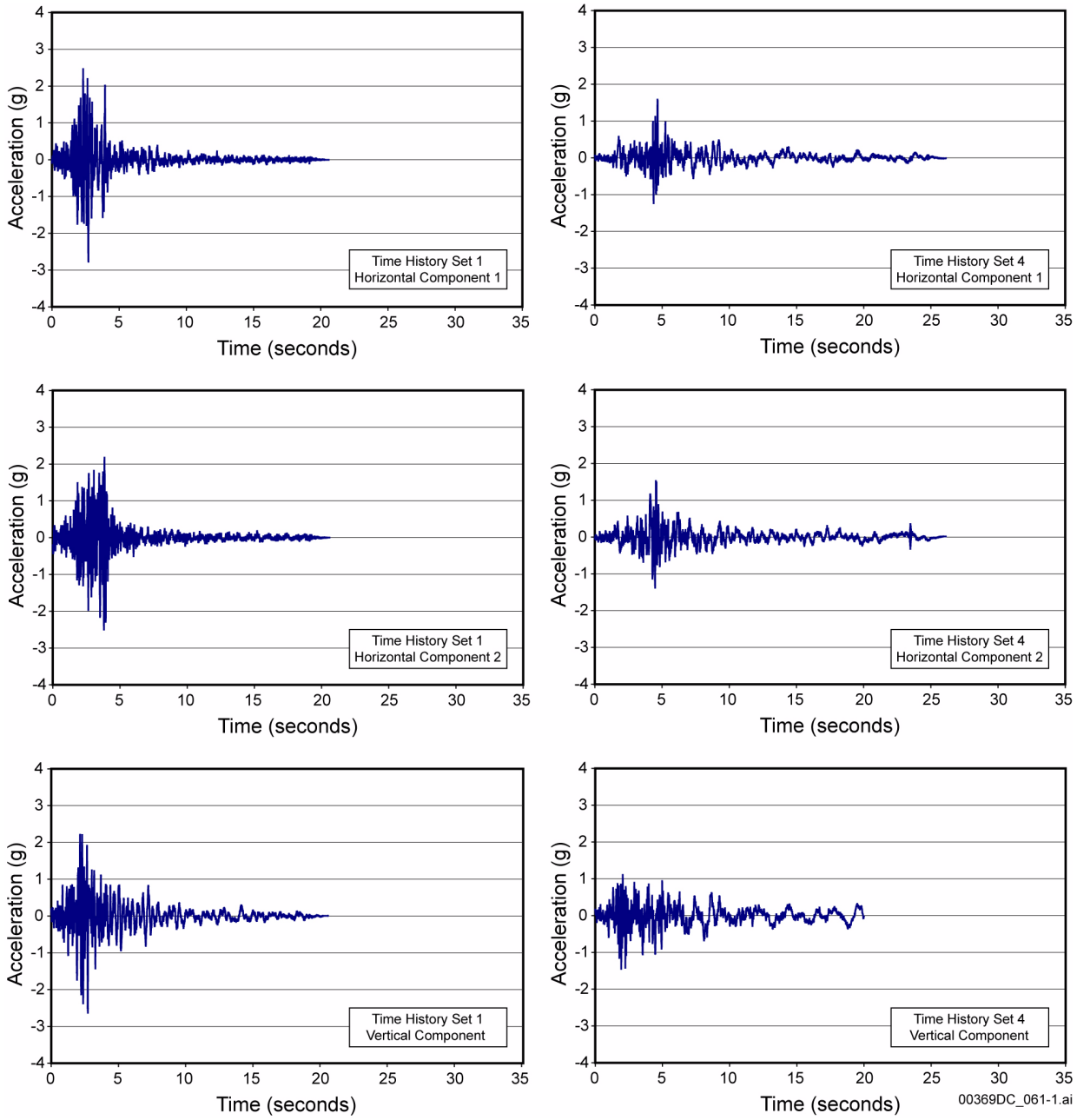

Figure 2.3.4-10. Example Time Histories with an Annual Exceedance Probability of 10^{-5} for the Waste Emplacement Level: Spectrally Conditioned to the Waste Emplacement Level and Scaled to Peak Ground Velocity

Source: BSC 2004b, Figures II-247 to II-249 and II-256 to II-258.

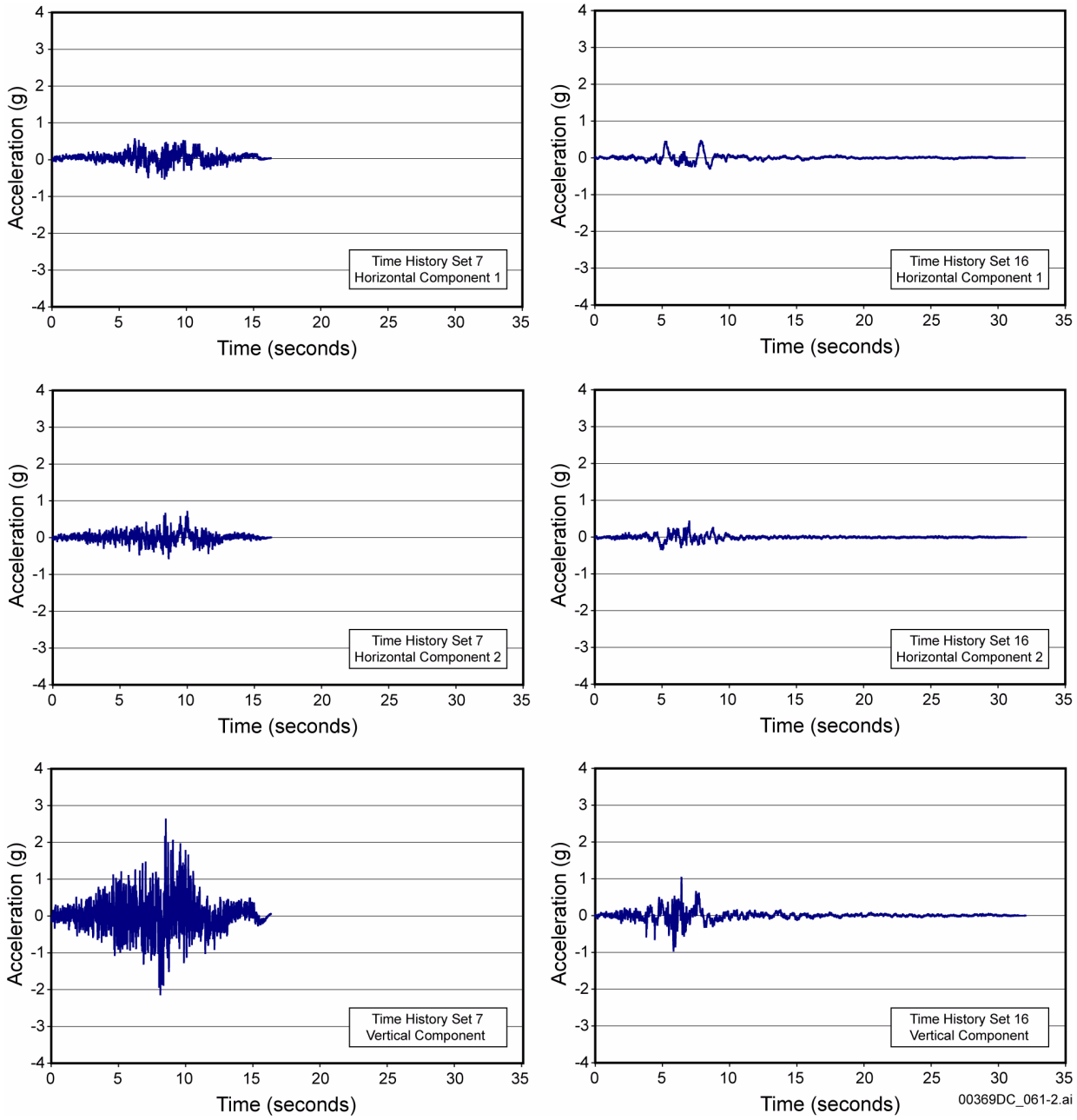

Figure 2.3.4-11. Example Time Histories with an Annual Exceedance Probability of 10^{-5} for the Waste Emplacement Level: Spectrally Conditioned to the Waste Emplacement Level and Scaled to Peak Ground Velocity

Source: BSC 2004b, Figures II-265 to II-267 and II-292 to II-294.

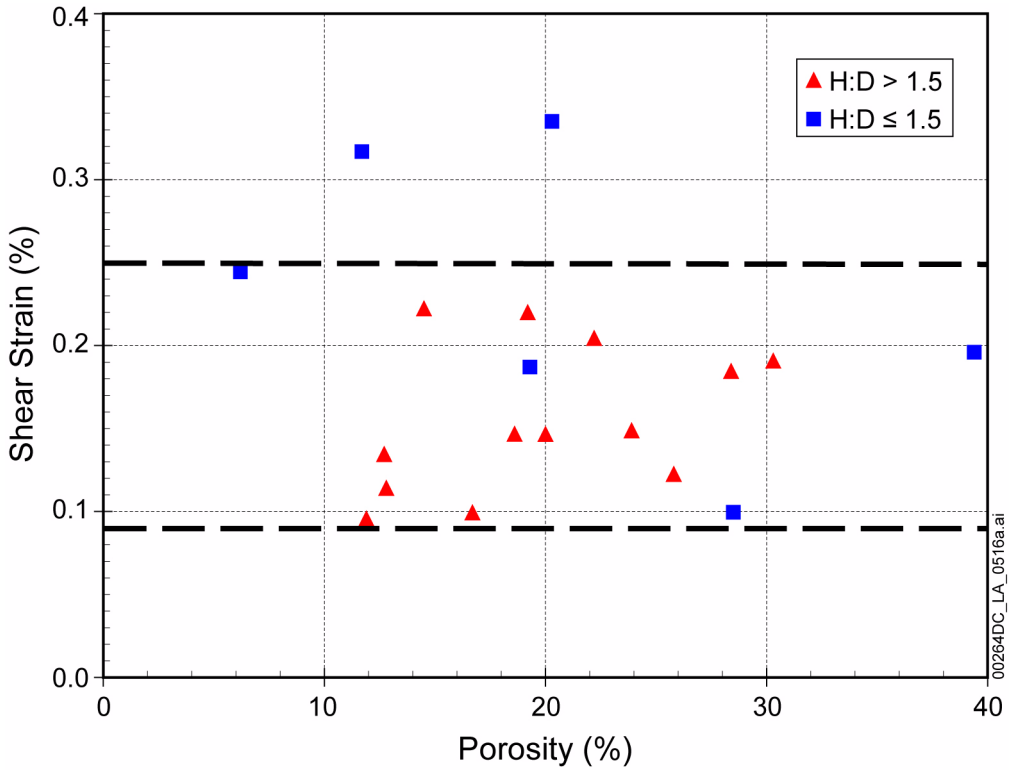

Figure 2.3.4-12. Shear-Strain Increment Determined for 288-mm Samples of Topopah Spring Tuff Lithophysal Rock

NOTE: Data are plotted as a function of lithophysal porosity. H:D indicates the height-to-diameter ratio of the sample tested. Data represent in situ conditions at 250-m depth.

Source: BSC 2005a, Figure 6-5.

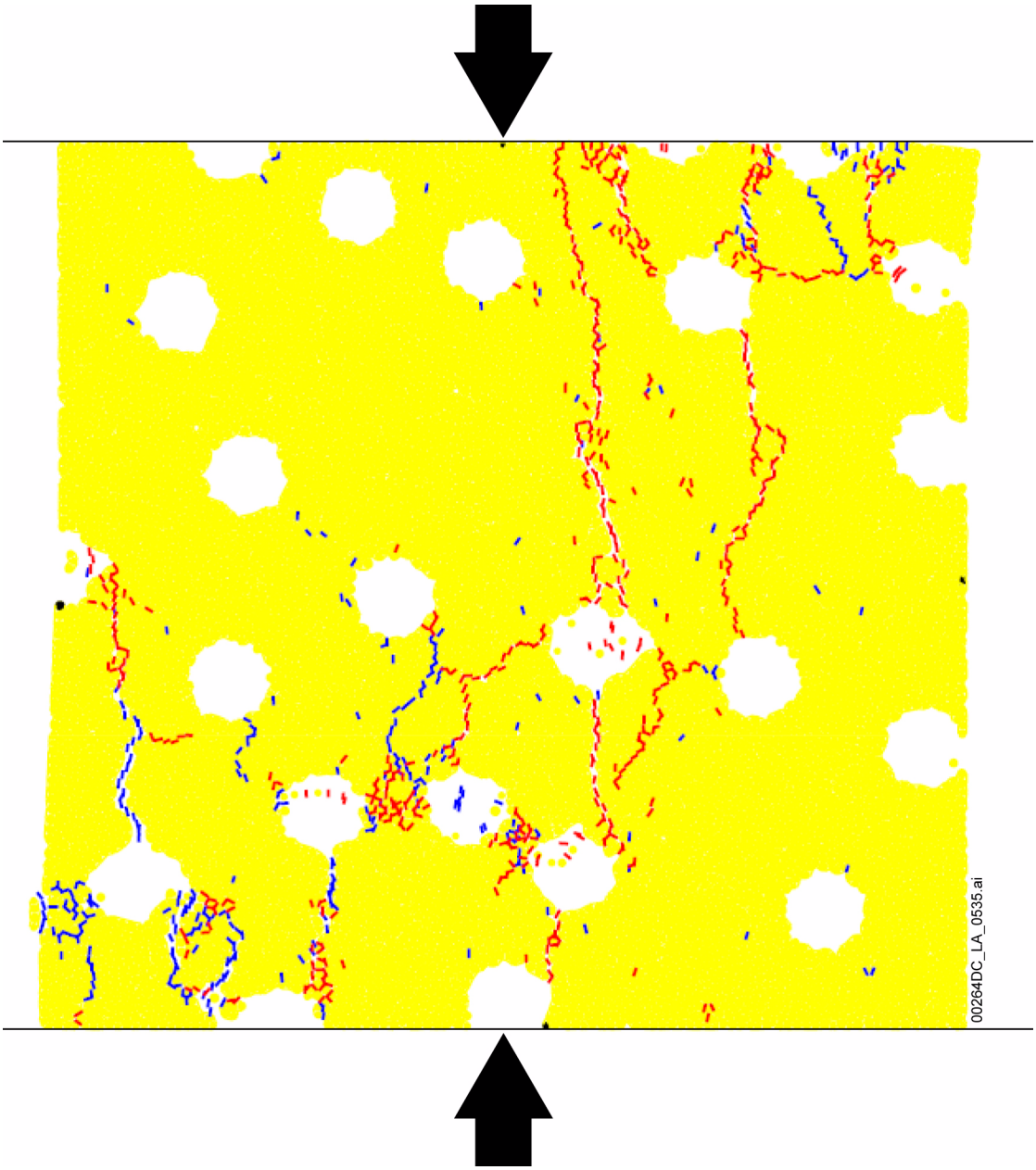

Figure 2.3.4-13. Example of Numerical Simulation of Lithophysal Rock Deformation

NOTE: Results shown are for a numerical simulation of unconfined compression test using the computer code PFC2D. Blue fractures are those that develop before the peak stress is reached; red fractures develop after peak stress is reached. Circular voids representing lithophysae are 90 mm in diameter. Blocks are 1 m × 1 m in dimension. Pressure was applied at the top and bottom boundaries.

Source: BSC 2005a, Figure 6-4.

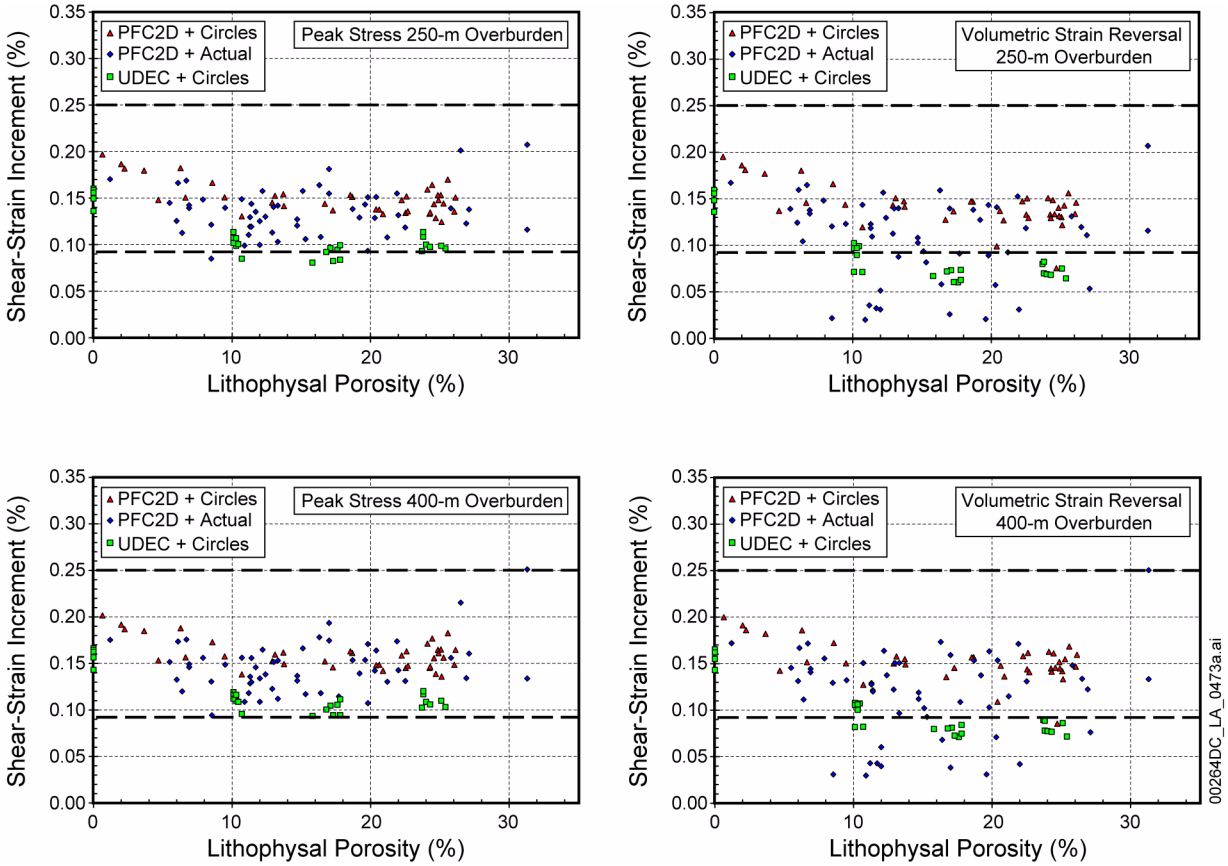

Figure 2.3.4-14. Shear-Strain Increment Plotted as a Function of Lithophysal Porosity as Determined from Numerical Simulation of Compression Testing of Topopah Spring Tuff

NOTE: Shear-strain increments are provided based on numerical simulation results from two software programs (PFC2D, UDEC) for two failure criteria (peak stress, volumetric strain reversal) and two depth levels below ground that span repository depth range (250 m and 400 m). The bold horizontal dashed lines correspond to the bounds of the shear-strain threshold probability distribution given in Figure 2.3.4-12.

Source: BSC 2005a, Figures B-8 to B-11.

INTENTIONALLY LEFT BLANK

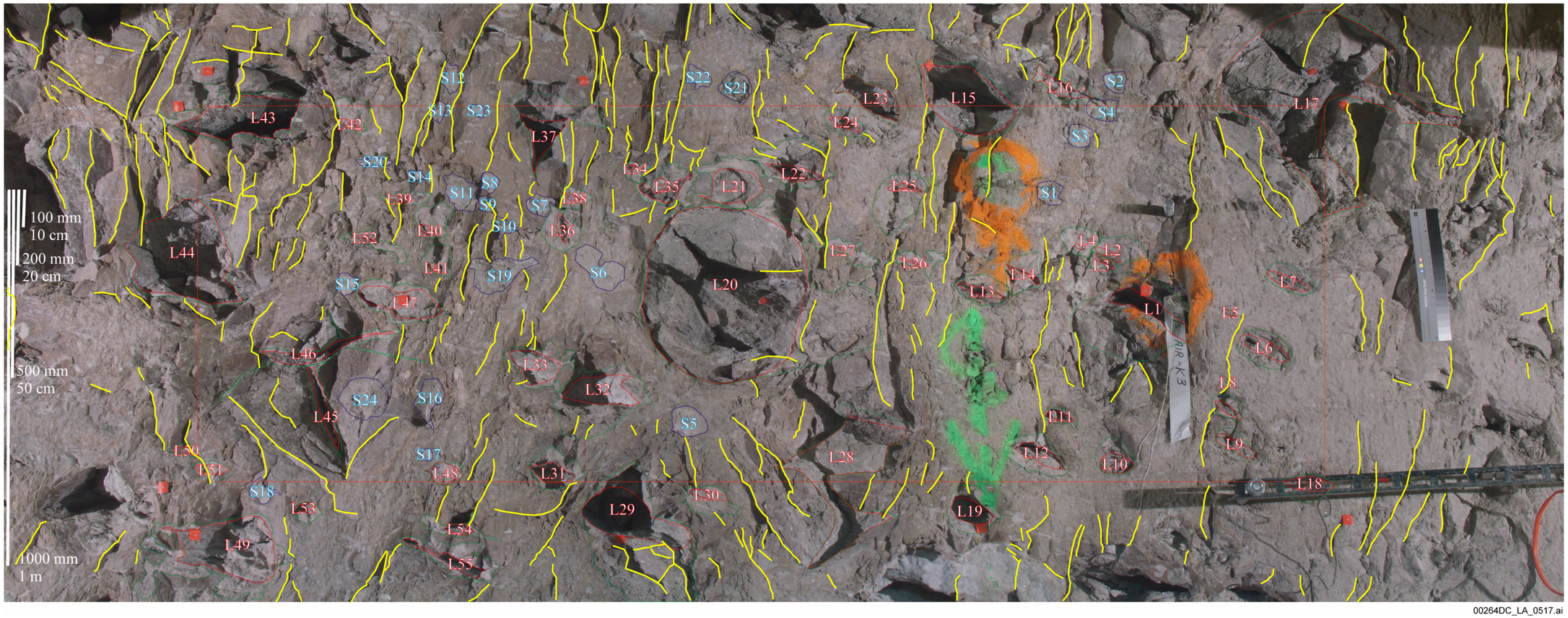

00264DC_LA_0517.ai

Figure 2.3.4-15. An Example 1-m-by-3-m Panel Map from the Lower Lithophysal Zone in the ECRB Cross-Drift Showing Lithophysae and Cooling Fractures

NOTE: Fractures are highlighted by yellow lines. Lithophysae are labeled "L," and spots (unformed lithophysae), "S.

Source: BSC 2005a, Figure 6-3.

INTENTIONALLY LEFT BLANK

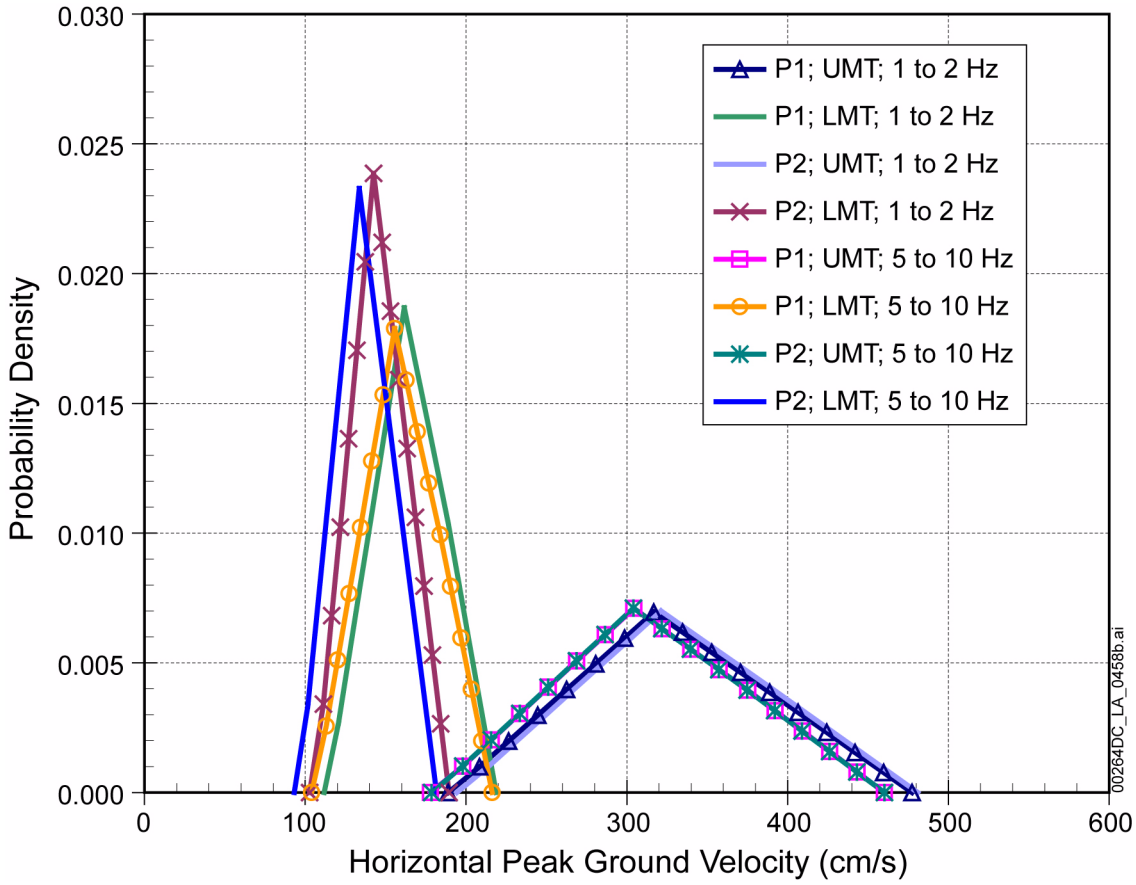

Figure 2.3.4-16. Probability Density Functions for the Bound to Horizontal Peak Ground Velocity at the Waste Emplacement Level

NOTE: In the legend, the notations refer to the various combinations of repository block velocity profiles (P1 and P2), dynamic material property curves (upper mean tuff (UMT) and lower mean tuff (LMT)), and response spectrum frequency range (1 to 2 Hz and 5 to 10 Hz).

Source: BSC 2005a, Figure 6-8.

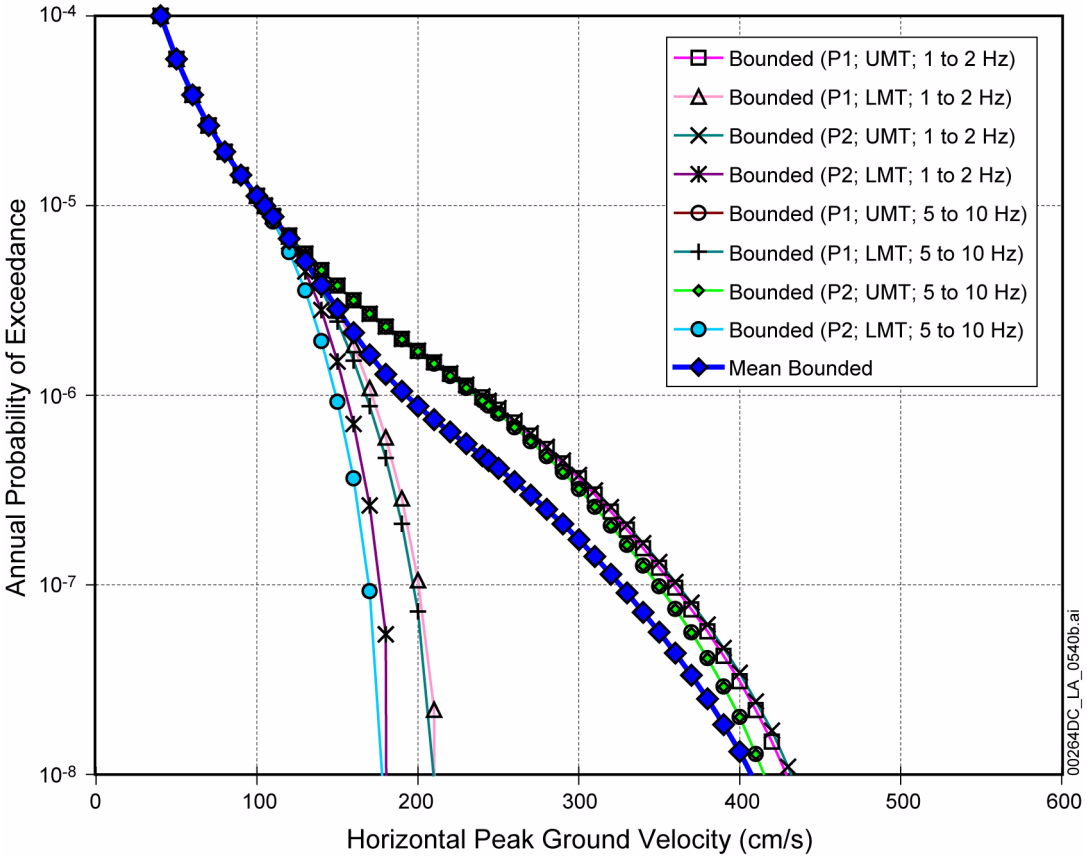

Figure 2.3.4-17. Individual and Average Bounded Peak Ground Velocity Hazard Curves for the Waste Emplacement Level

NOTE: The eight individual PGV hazard curves reflect the eight site-response modeling cases. These cases represent combinations of velocity profiles and dynamic material property curves used as input to the site-response model and also two ranges of spectral response frequency. The different velocity profiles and dynamic material property curves reflect the epistemic uncertainty included in the site response modeling. LMT = lower mean tuff dynamic material property curve; P1 = base-case velocity profile 1; P2 = base-case velocity profile 2; UMT = upper mean tuff dynamic material property curve.

Source: BSC 2005a, Figure 6-9.

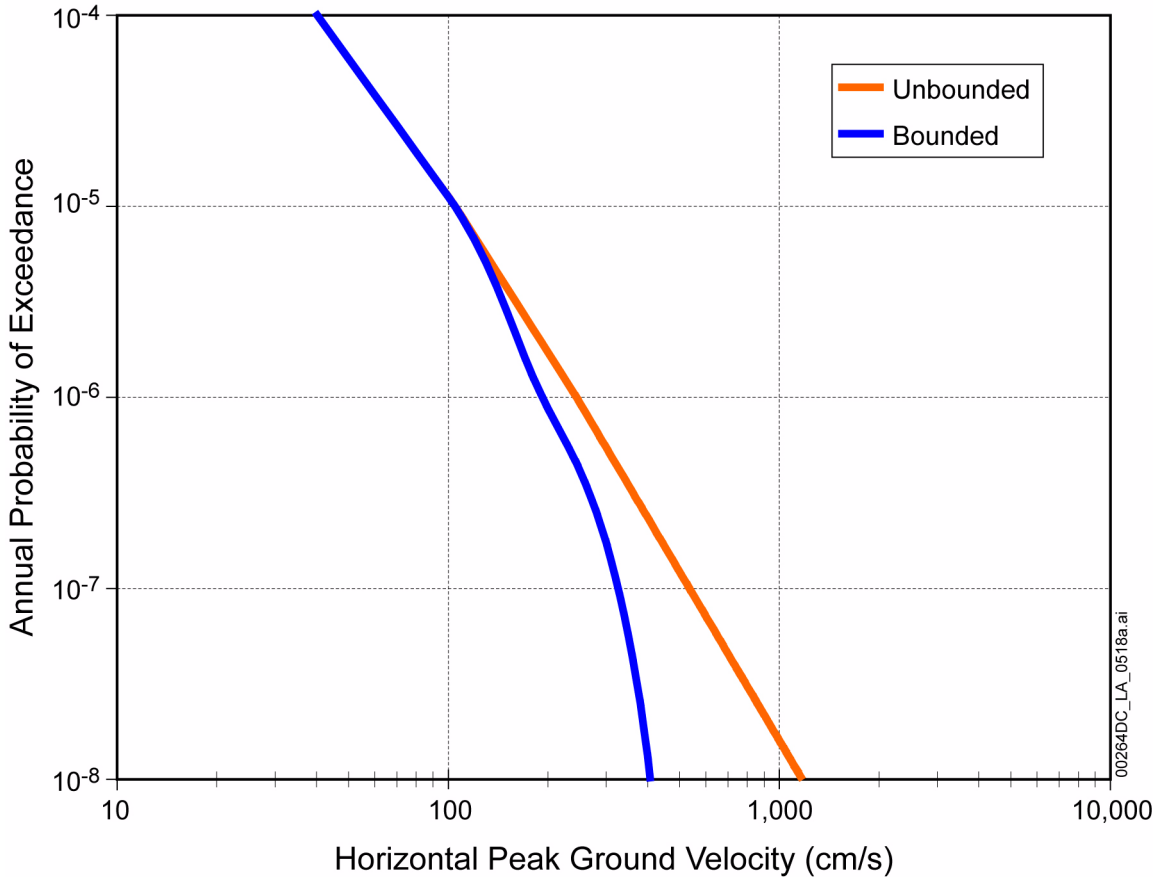

Figure 2.3.4-18. Horizontal Peak Ground Velocity Mean Hazard Curves for Bounded and Unbounded Ground Motion at the Waste Emplacement Level

Source: BSC 2005a, Figure 6-10.

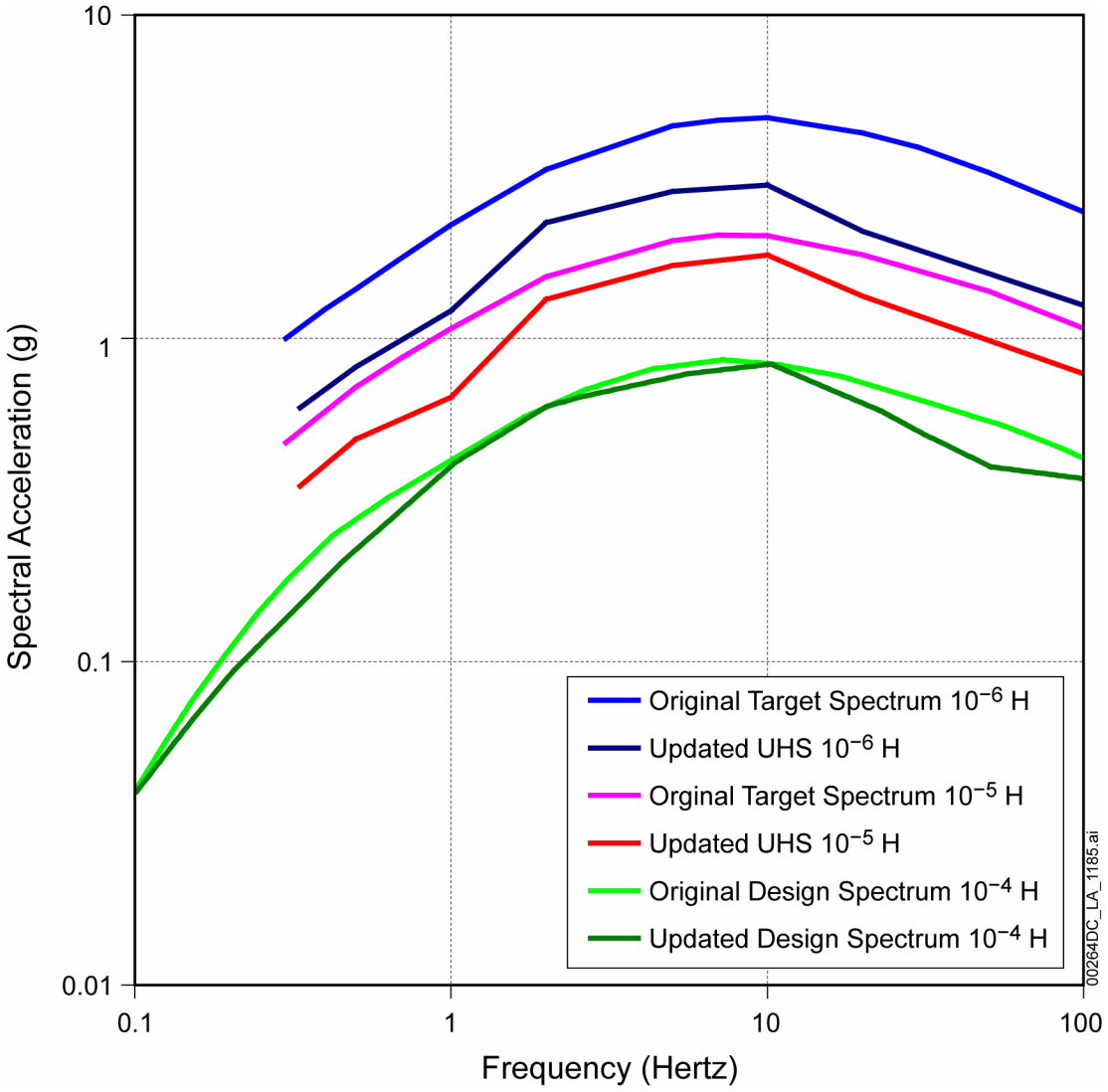

Figure 2.3.4-19. Comparison of Response Spectra Using Different Inputs and Approaches

Source: Original target spectra and original design spectrum, BSC 2004b (10^{-4}, Figure 6.3-16; 10^{-5}, Figure 6.3-42; 10^{-6}, Figure 6.3-47); updated uniform hazard spectra and updated design spectrum, BSC 2008 (10^{-4}, Figure 6.5.3-33; 10^{-5}, Figure 6.5.3-22; 10^{-6}, Figure 6.5.3-23).

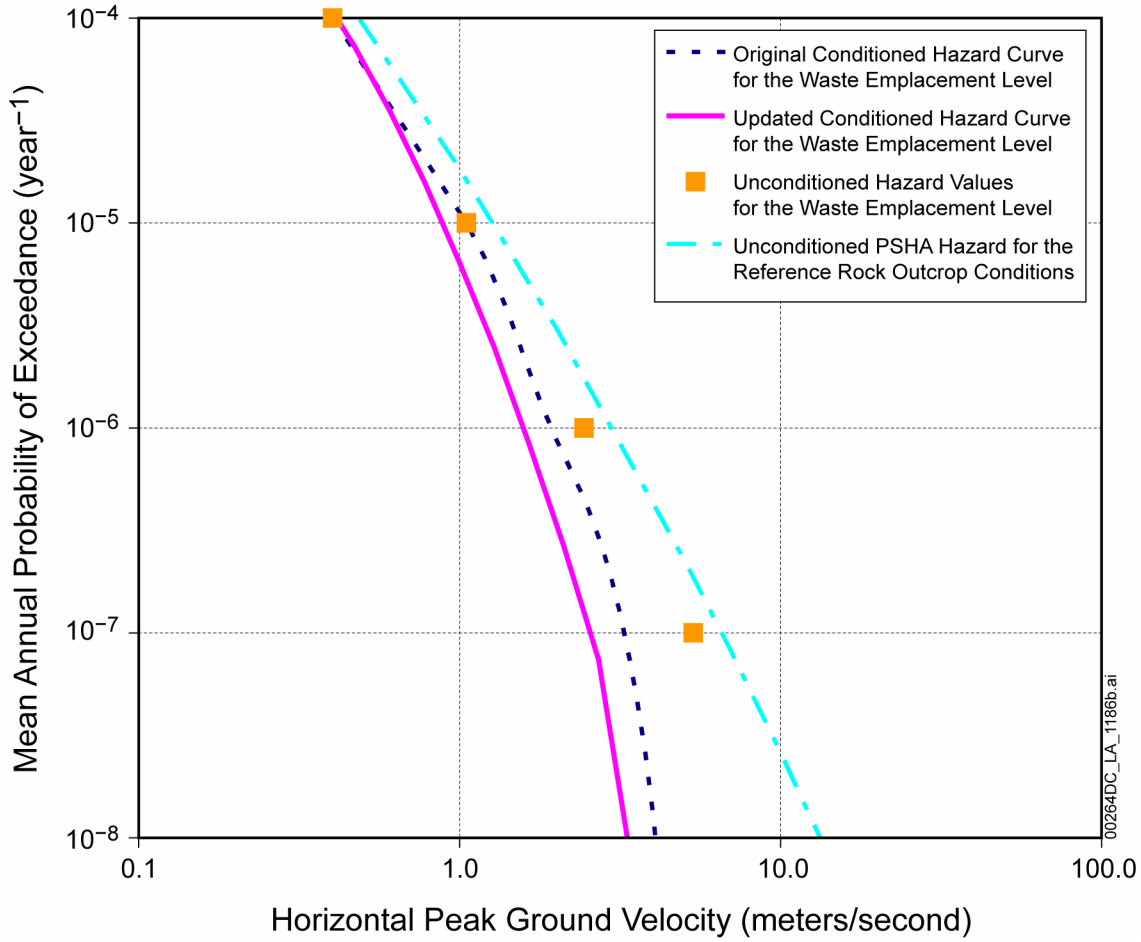

Figure 2.3.4-20. Comparison of Horizontal PGV Hazard at the Waste Emplacement Level

Source: Unconditioned hazard curve for the PSHA reference rock outcrop conditions, BSC 2004b, Figure 6.2-4; other data BSC 2008, Figure 6.5.3-17b.

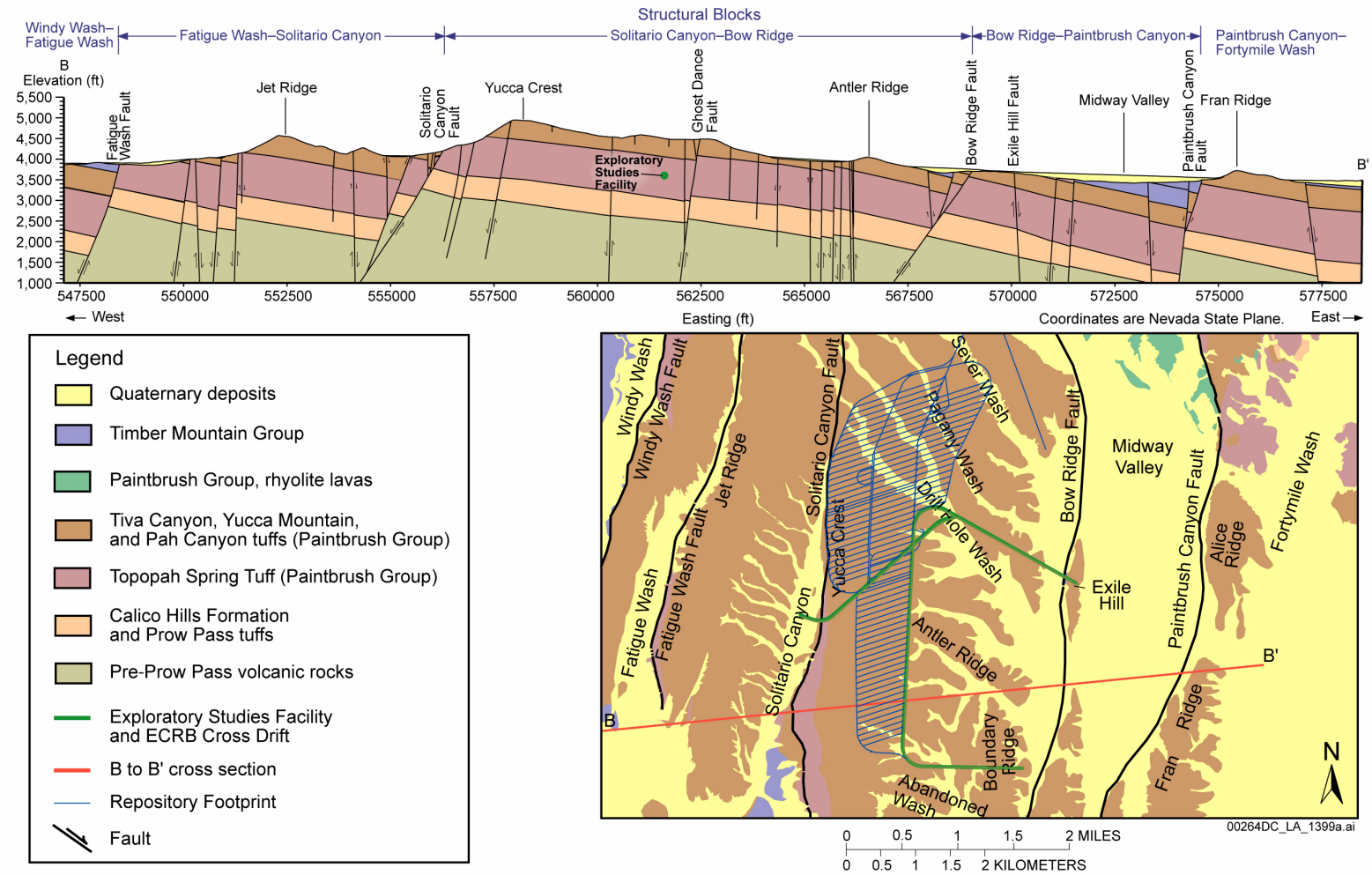

Figure 2.3.4-21. Approximate East–West Geologic Section across Yucca Mountain Site Area (top) along Line of Cross Section in Plan View (bottom)

NOTE: Location of intersection along line of section.

Source: Day et al. 1998, cross section B-B; Potter et al. 2002, plan view.

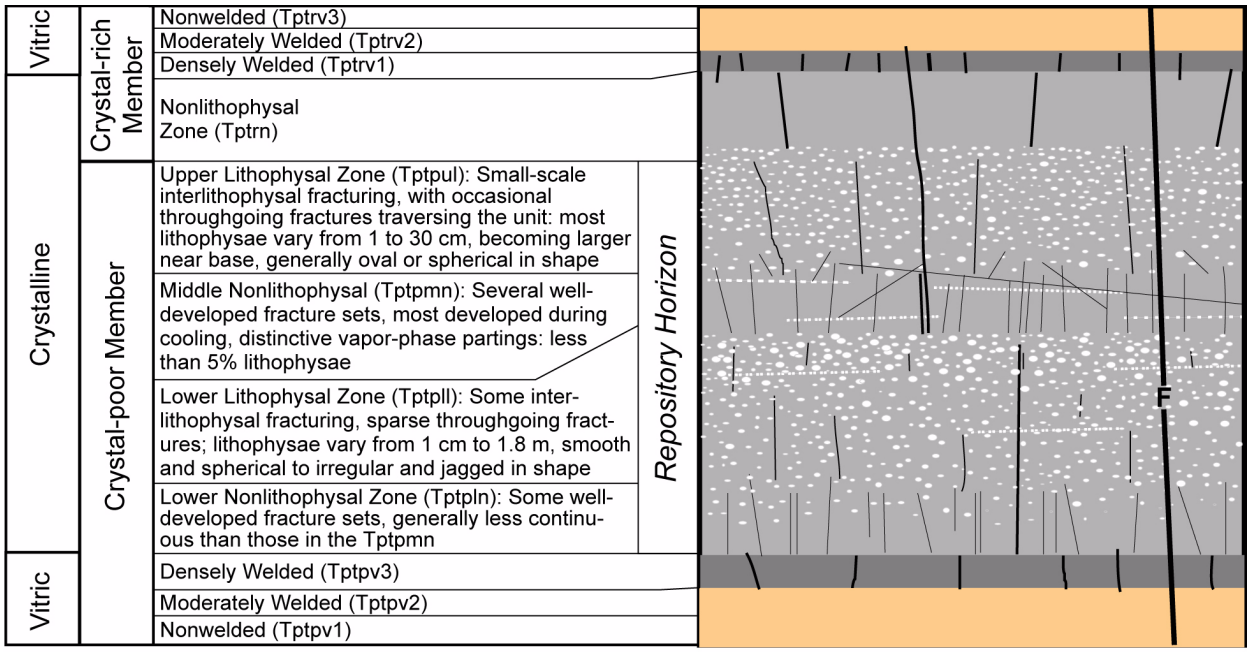

Diagrammatic Cross Section of the Topopah Spring Tuff Illustrating Relative Discontinuity Densities and Orientations: This figure indicates how fractures, faults, and lithophysae are typically distributed through the ignimbrite.

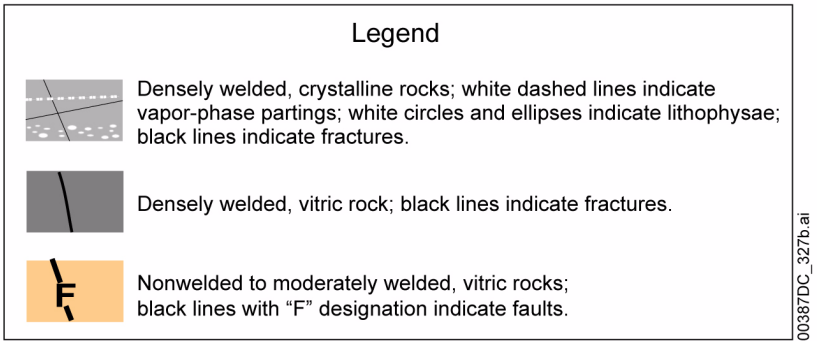

Figure 2.3.4-22. Schematic Illustration of the Structure of the Topopah Spring Member

NOTE: Stratigraphic nomenclature after Day et al. (1998).

Source: BSC 2004a, Figure 6-4.

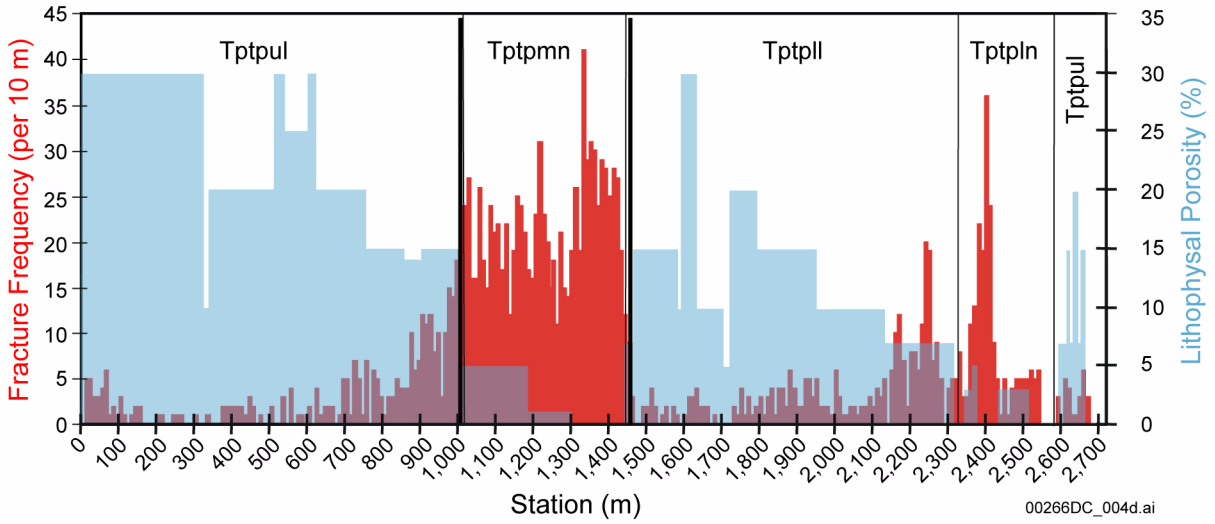

Figure 2.3.4-23. Composite Plot of Fracture Frequency for Fractures with Trace Lengths Greater than 1 m and Lithophysal Porosity as a Function of Distance along the Enhanced Characterization of the Repository Block Cross-Drift

NOTE: There is an inverse relationship between fracture density and lithophysal porosity.

Source: Mongano et al. 1999.

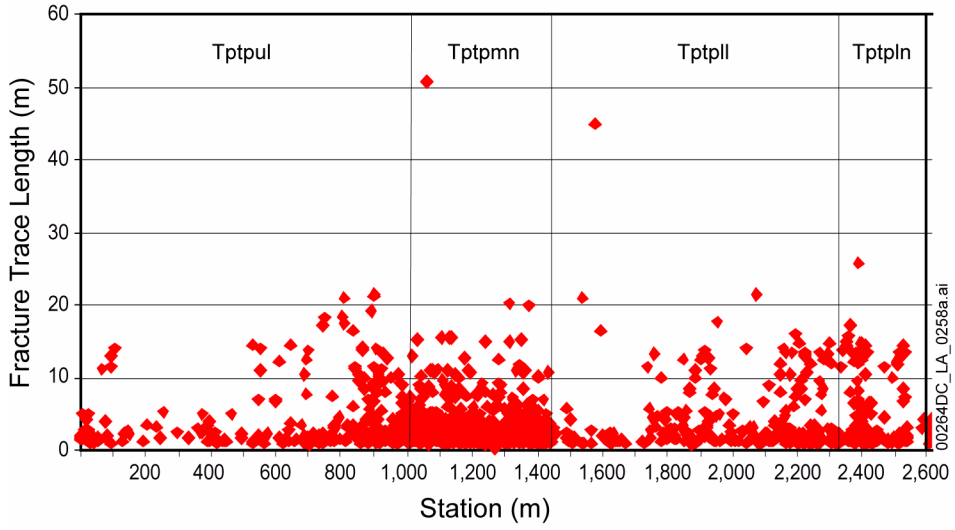

Figure 2.3.4-24. Fracture Trace Length as a Function of Distance along the Enhanced Characterization of the Repository Block Cross-Drift and by Subunit of the Crystal Poor Member of the Topopah Spring Tuff from Detailed Line Surveys

Source: BSC 2004a, Figure 6-6.

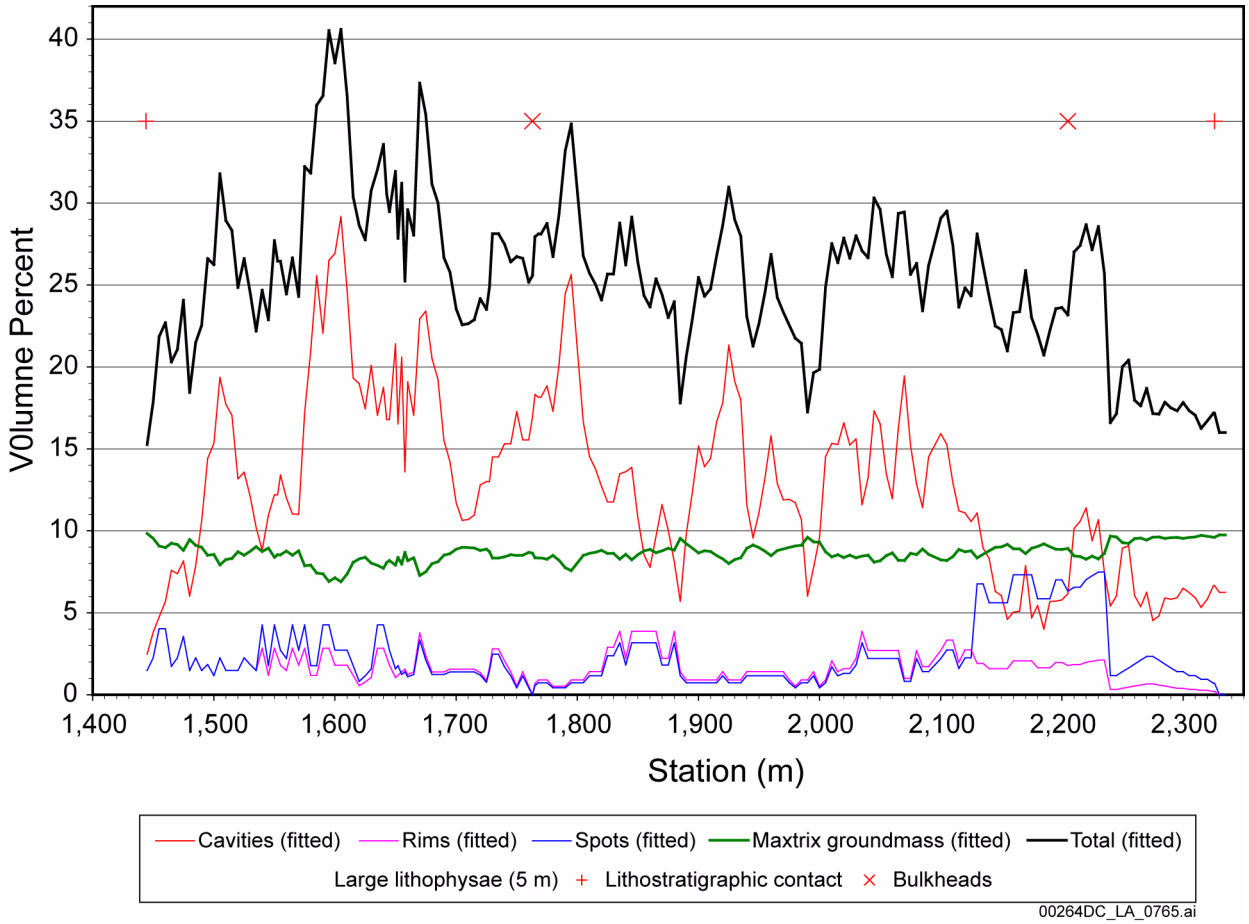

Figure 2.3.4-25. Calculated Porosity of Lithophysal Cavities, Rims, Spots, Matrix Groundmass, and the Total Porosity in the Tptpll Exposed along the Enhanced Characterization of the Repository Block Cross-Drift

NOTE: The term “spots” refers to crystallized material similar to rims on a lithophysal cavity. Rather than an open void, the spot is composed of crystallized material with a porosity higher than the surrounding matrix groundmass.

Source: BSC 2004a, Appendix O, Figure O-15(a).

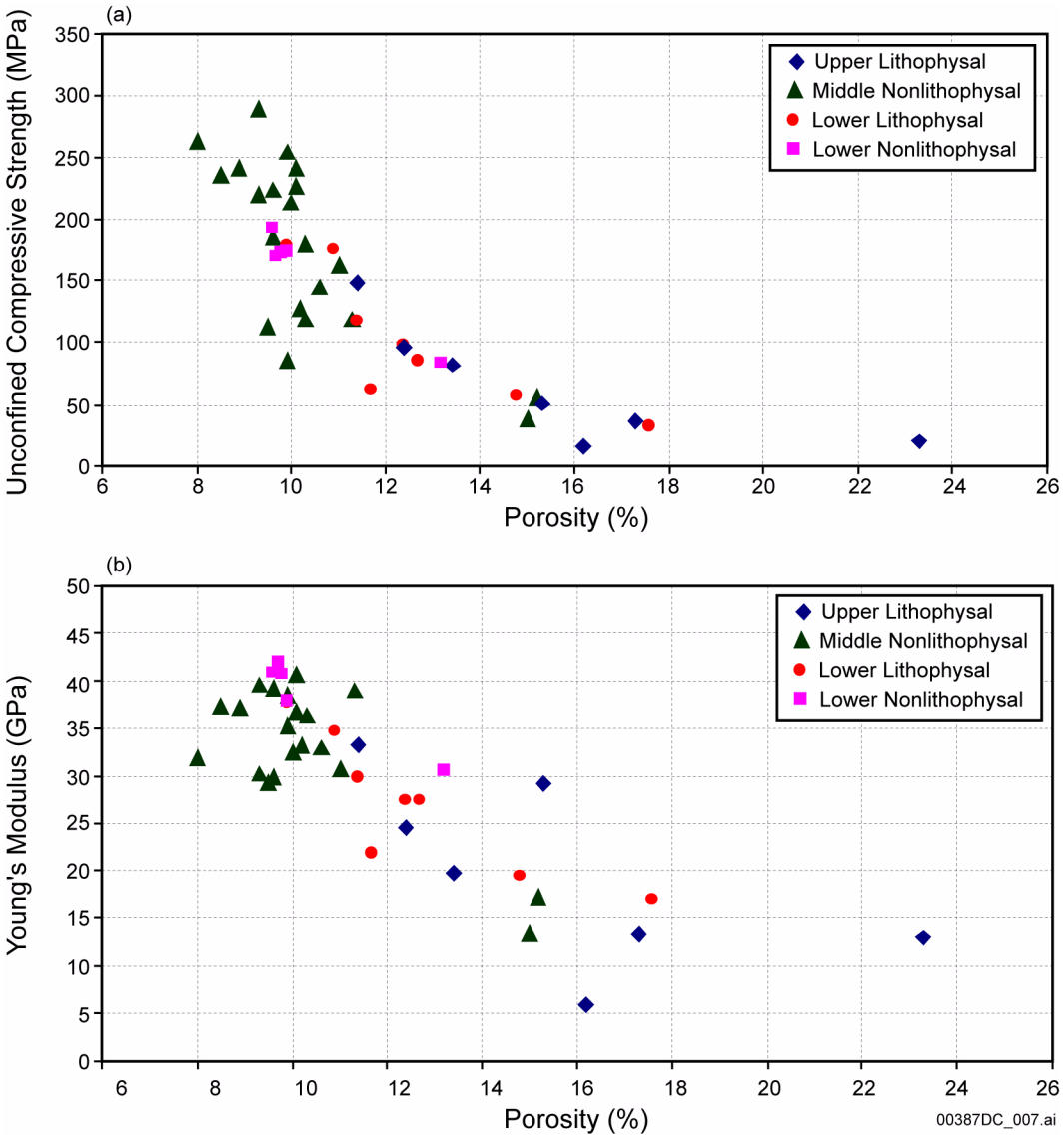

Figure 2.3.4-26. Intact Unconfined Compressive Strength and Young's Modulus for Topopah Spring Subunits as a Function of Effective Porosity

NOTE: Porosity is composed of matrix and lithophysal porosity. All measurements are from a 50.8-mm-diameter core, saturated, at room temperature, length to diameter ratio = 2:1, and a strain rate of 10^{-5} per second. Small cores from lithophysal zones generally contain only small amounts of lithophysal porosity, and thus the above tests are not indicative, in general, of properties of the lower and upper lithophysal units.

Source: BSC 2004a, Appendix E, Figure E-3.

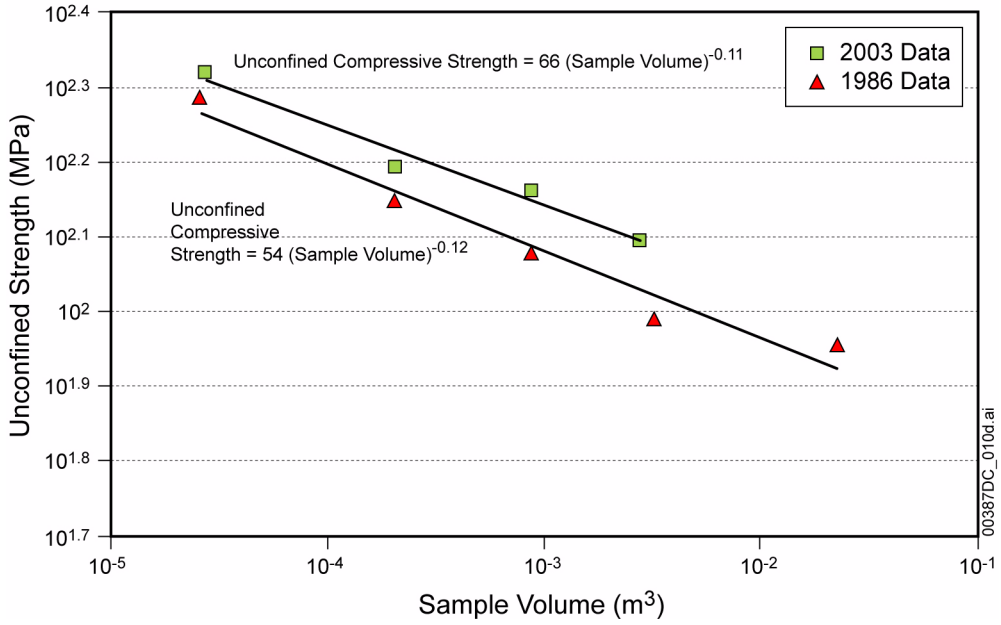

Figure 2.3.4-27. Results of Size Effect Study Showing Variation in Sample Unconfined Compressive Strength as a Function of Sample Volume

NOTE: Results from the 2003 testing of Tptpln and Tptpll samples (BSC 2004a, Appendix E) are compared to previous testing (1986) of samples from the Tptpmn (Price 1986).

Source: BSC 2004a, Appendix E, Figure E-20.

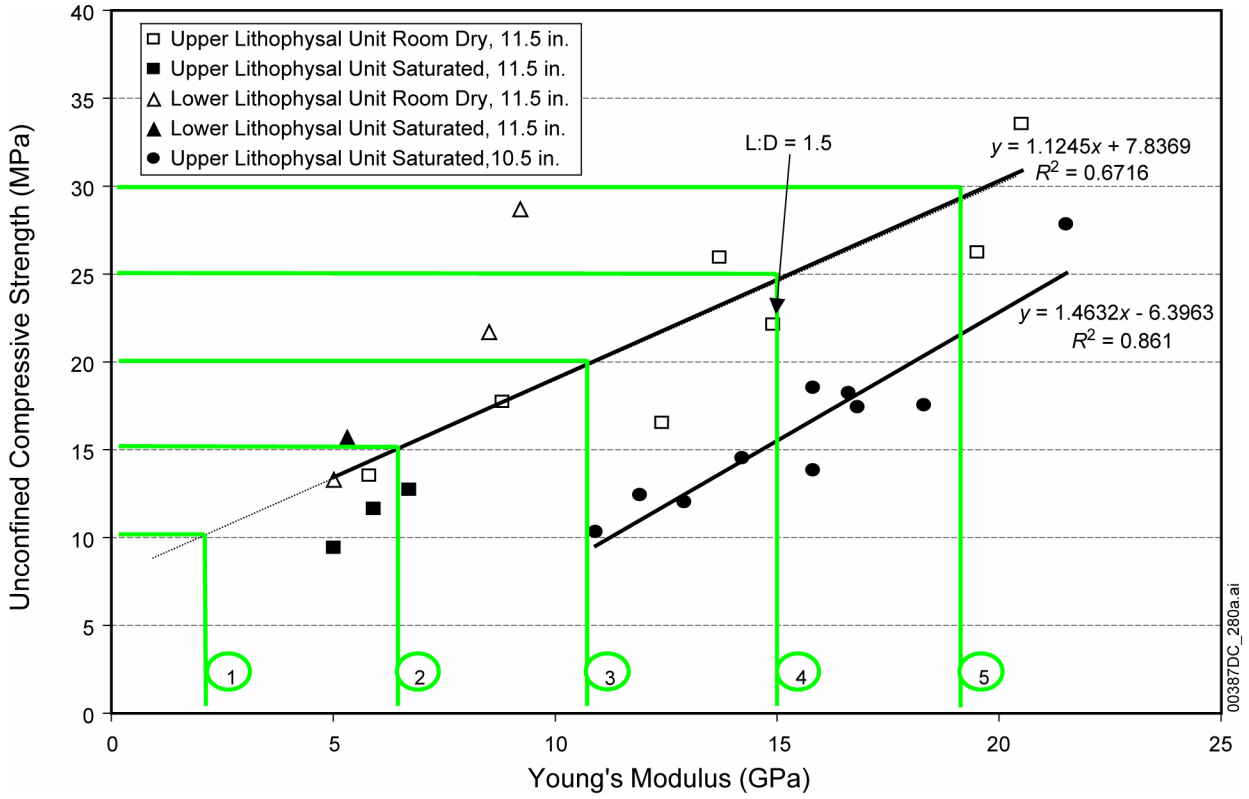

Figure 2.3.4-28. Relationship of Unconfined Compressive Strength to Young's Modulus from Large Core Testing of Lithophysal Rock and Assignment of Five Average Quality Categories

NOTE: Base-case strength and modulus data used in rockfall analysis are based on fit to 11.5-in. core data. See Figure 2.3.4-30 for bounding ranges.
L:D = length:diameter ratio.

Source: BSC 2004a, Appendix E, Figure E-8.

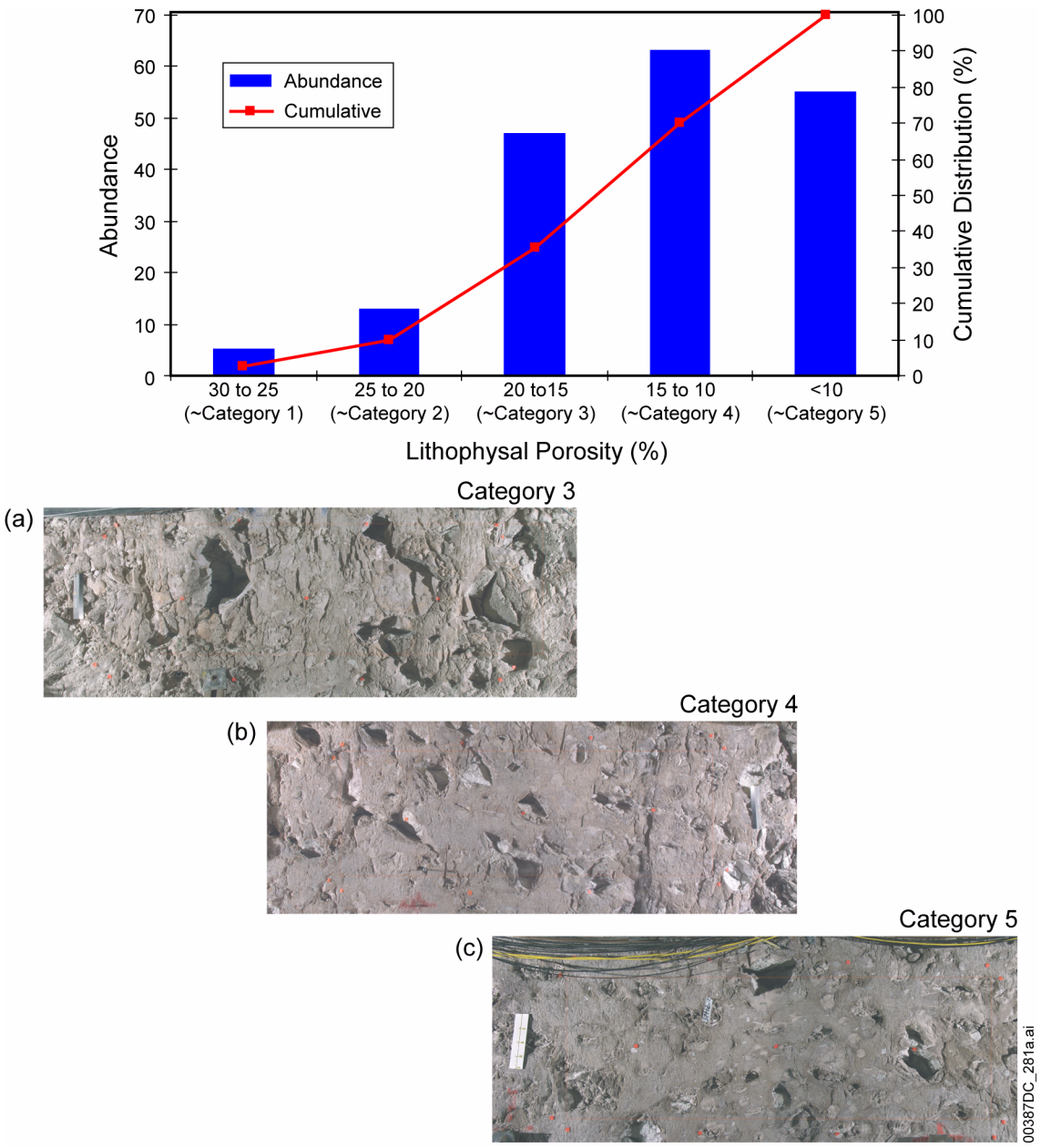

Figure 2.3.4-29. Distribution of Lithophysal Porosity and Estimated Rock Properties Categories for the Tptpll in the Enhanced Characterization of the Repository Block Cross-Drift

NOTE: Lithophysal porosity abundance data in histogram are from ECRB Cross-Drift stations 14+44 to 23+26. Shown are examples of approximate rock strength category levels taken from 1-by-3-m panel maps: Category 3 (a) with lithophysal porosity of approximately 19%, Category 4 (b) with lithophysal porosity of 13.3%, and Category 5 (c) with lithophysal porosity of 8.5%.

Source: BSC 2004a, Appendix E, Figures E-9 and E-10.

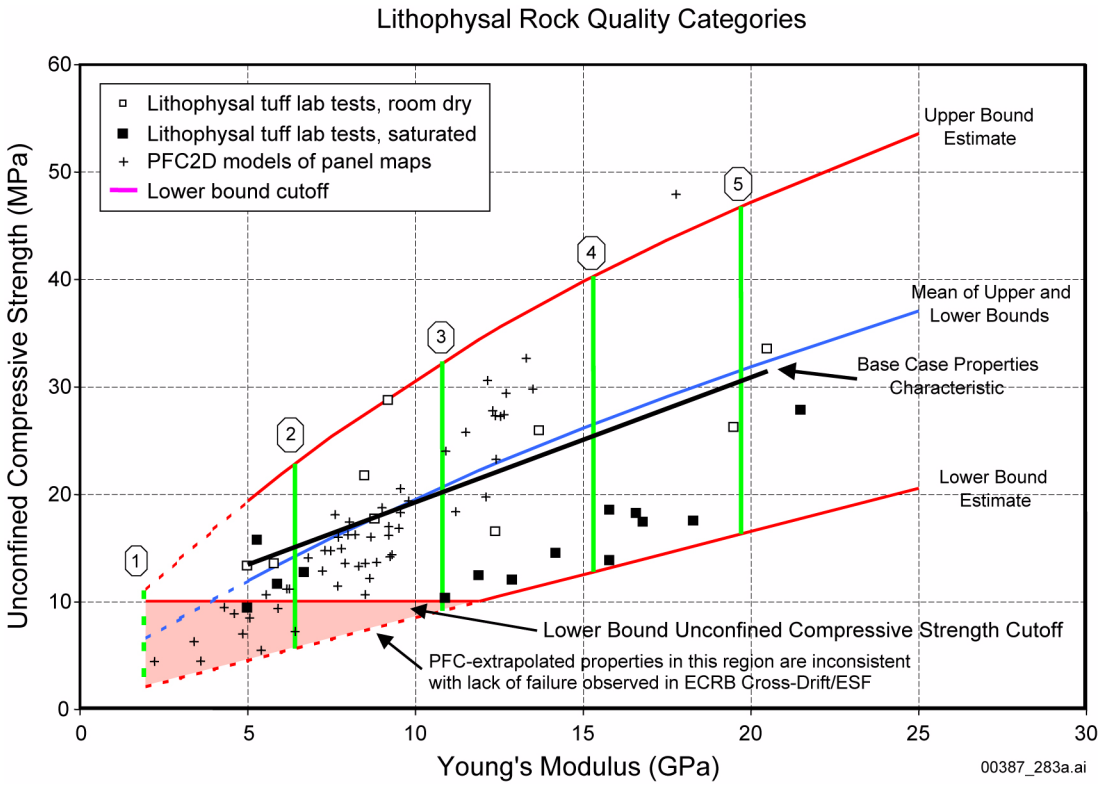

Figure 2.3.4-30. Estimated Upper and Lower Bounds of Unconfined Compressive Strength and Young's Modulus for Lithophysal Rock

NOTE: The five strength categories are shown with base-case properties and their ranges. Base-case properties were used in rockfall analyses; lower bounding ranges were examined in sensitivity studies. The bounding curves are empirically derived to include all large core laboratory data, including 267-mm diameter saturated cores from Busted Butte. Base-case properties characteristics, derived from 290-mm diameter cores, are also shown. Extrapolated (PFC) strength values below 10 MPa are localized and inconsistent with observations of lack of yielding in ECRB Cross-Drift and ESF.

Source: BSC 2004a, Appendix E, Figure E-13.

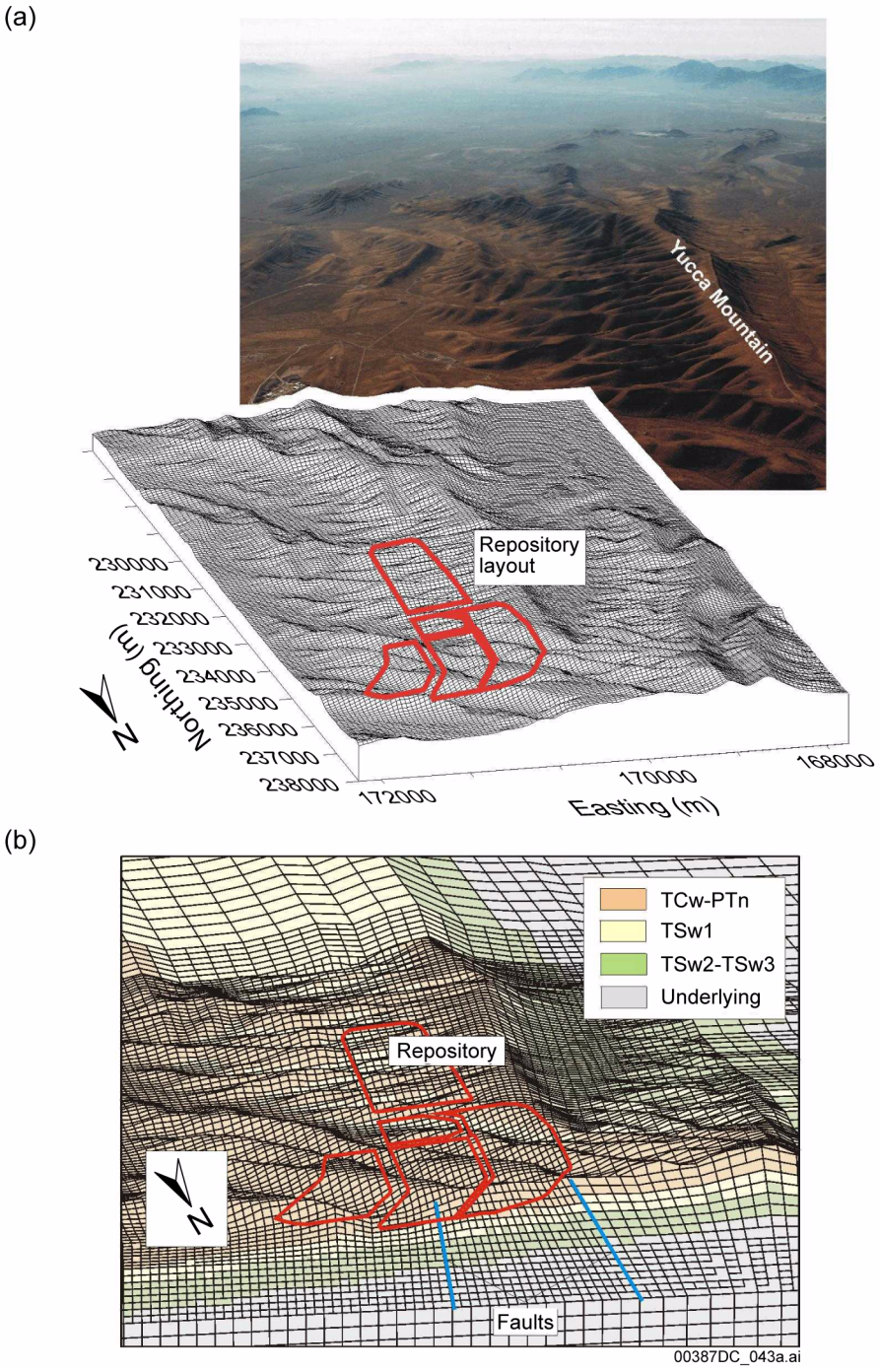

Figure 2.3.4-31. Aerial View of the Yucca Mountain Site and Digital Elevation Calculation Created from Topographic Information (a) and View of the Regional-Scale FLAC3D Thermal-Mechanical Model Constructed from the Digital Elevation Calculation and Available Geologic Information (b)

NOTE: (a) View is toward south. (b) Repository panel outline is superimposed.

Source: BSC 2004a, Appendix C, Figure C-1.

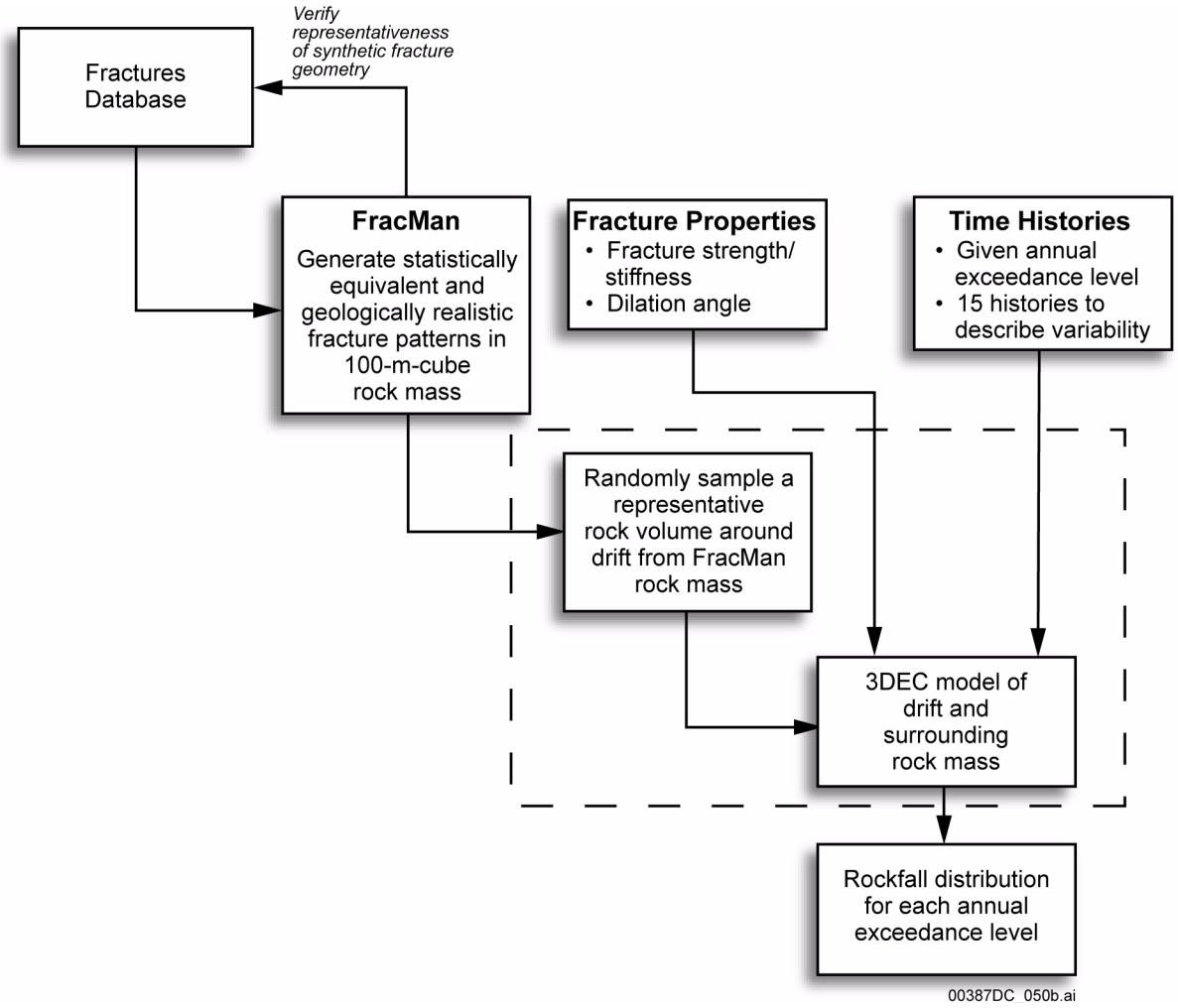

Figure 2.3.4-32. Approach to Analysis of Drift Degradation and Rockfall in Nonlithophysal Rock from Combined In Situ, Thermal, and Seismic Loading

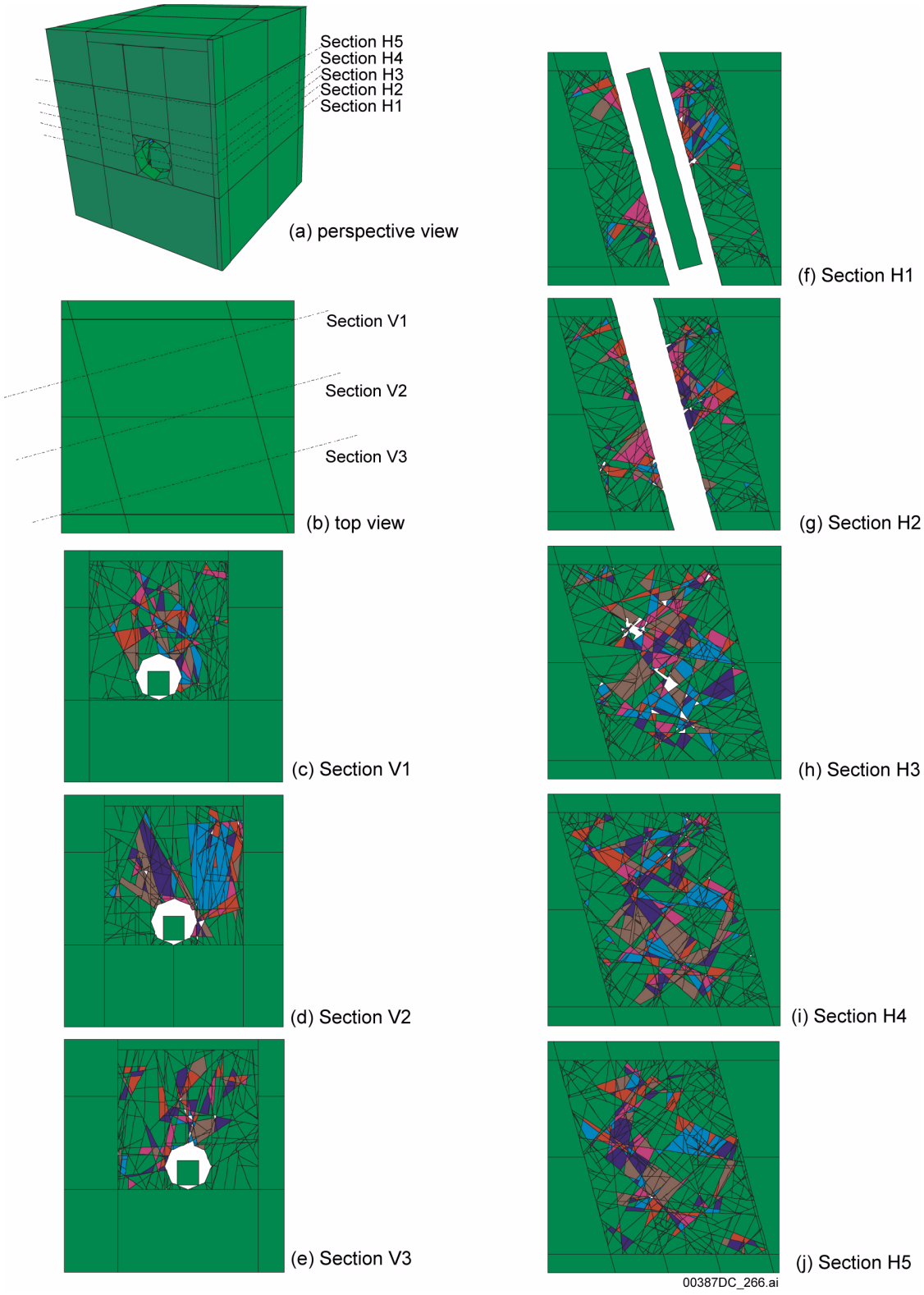

Figure 2.3.4-33. 3DEC Model Geometry and Cross Sections (a) to (e) and Plan View Sections (f) to (j) Showing the Internal Fracture Geometry as Imported from FracMan

Source: BSC 2004a, Figure 6-34.

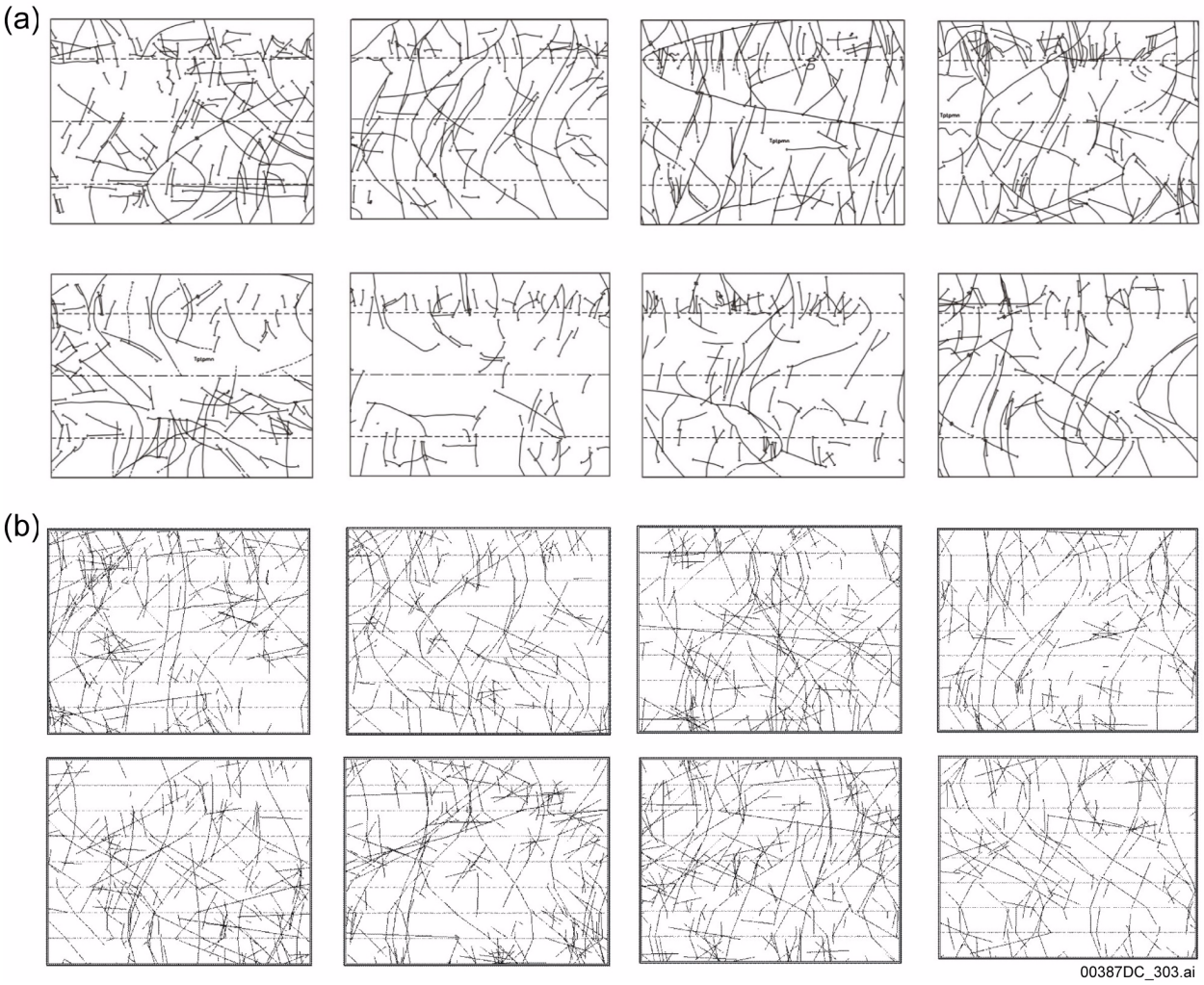

Figure 2.3.4-34. Comparison of (a) Full Periphery Geologic Fracture Maps from the Tptpmn in the Exploratory Studies Facility with (b) Simulated Full Periphery Geologic Fracture Maps from the FracMan Cube

NOTE: The full periphery map is a fracture trace map of the sidewalls and roof of the circular tunnel that has been laid flat and viewed from above. The purpose of this figure is to illustrate the geologic structure contained on a full periphery geologic map. The annotated information on this figure is not intended to be legible. Each map is 25 m in the horizontal direction. Only those fractures greater than 1 m in length are included on the fracture maps.

Source: BSC 2004a, Figure 6-21.

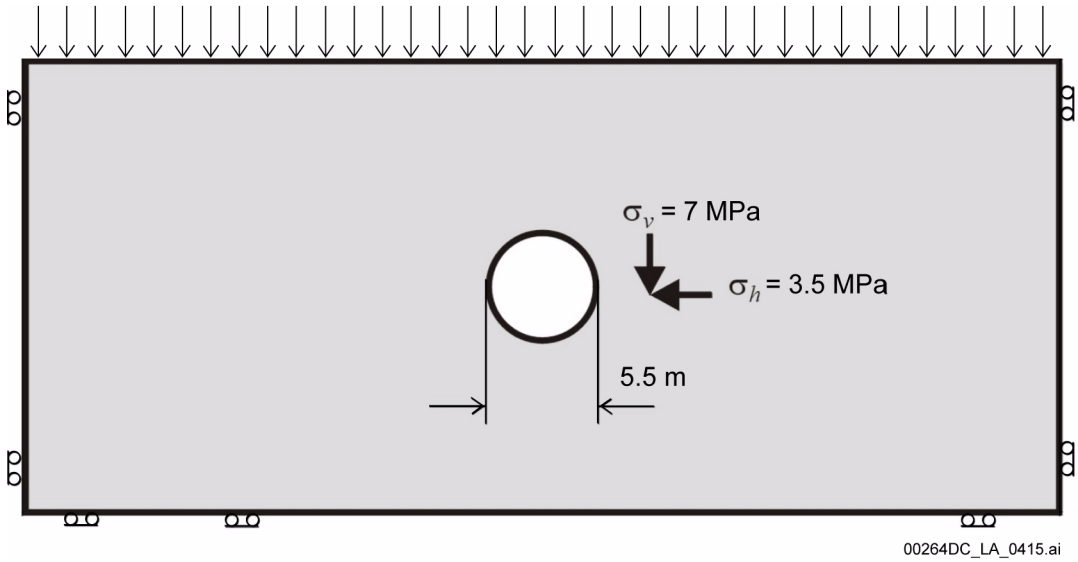

Figure 2.3.4-35. Schematic of Model Showing Initial and Boundary Conditions: Initial Static Simulation

NOTE: Surcharge on top of model equals the weight of the overlying rock mass.

Source: BSC 2004a, Figure 6-117.

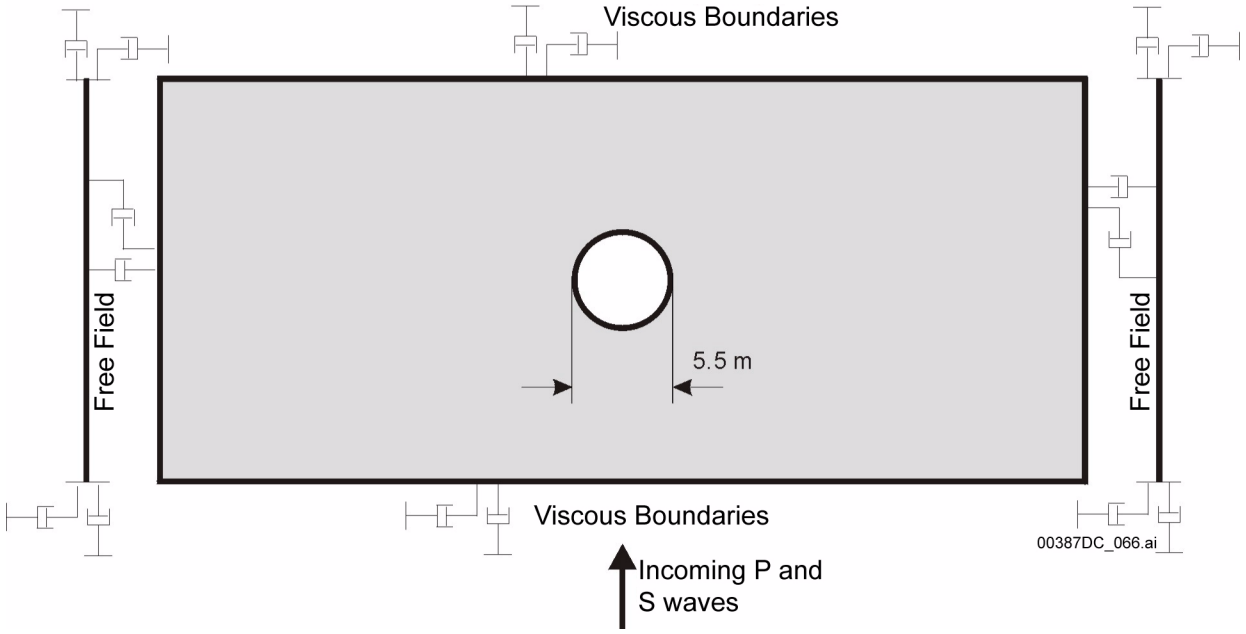

Figure 2.3.4-36. Schematic of Model Boundary Conditions for Dynamic Simulation

Source: BSC 2004a, Figure 6-118.

Figure 2.3.4-37. A Snapshot of a Simulation of Rockfall Impact to the Drip Shield, Nonlithophysal 3DEC Model

NOTE: The three-dimensional simulation shows rockfall in an emplacement drift. The individual rocks are seen impacting the rectangular block, which approximates the drip shield.

Source: BSC 2004a, Figure 6-49.

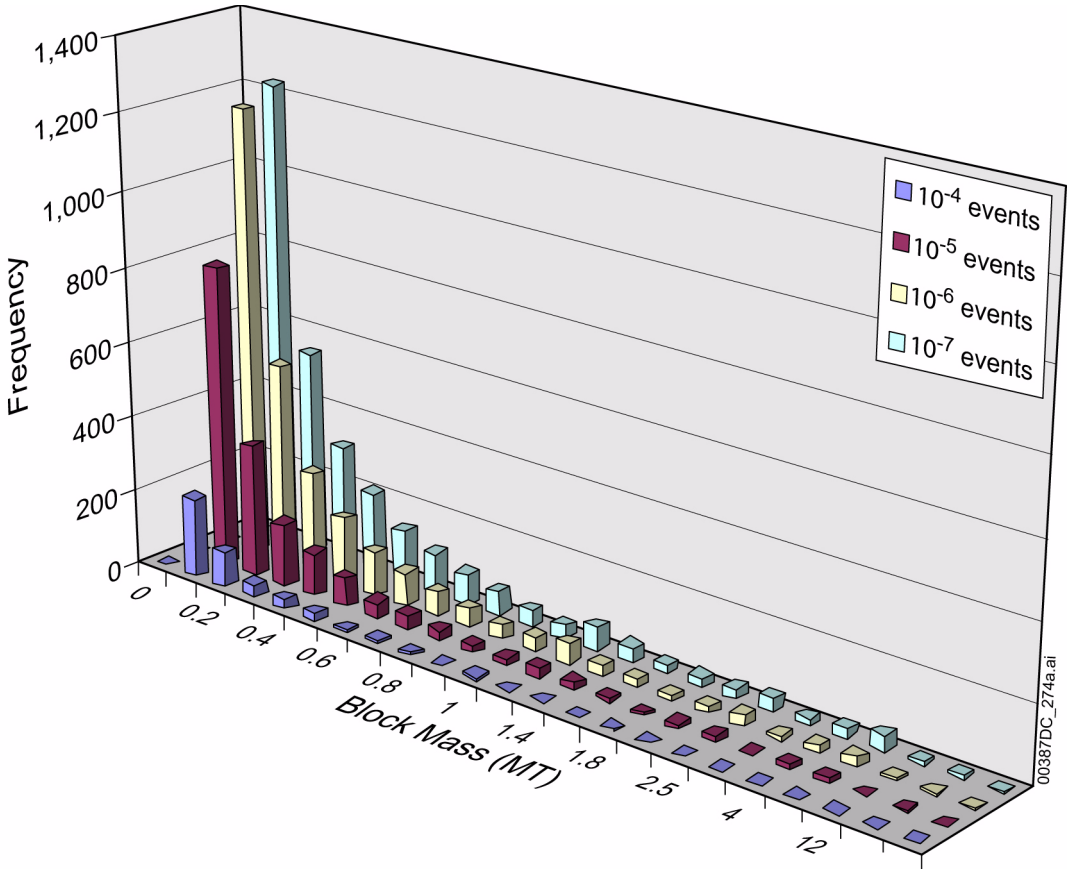

Figure 2.3.4-38. Comparison of Histograms of Rockfall Block Masses (in Metric Tons) from All Postclosure and Preclosure Seismic Analyses in Nonlithophysal Rock

NOTE: Block mass frequencies were determined using unbounded ground motions.

Source: BSC 2004a, Figure 6-81.

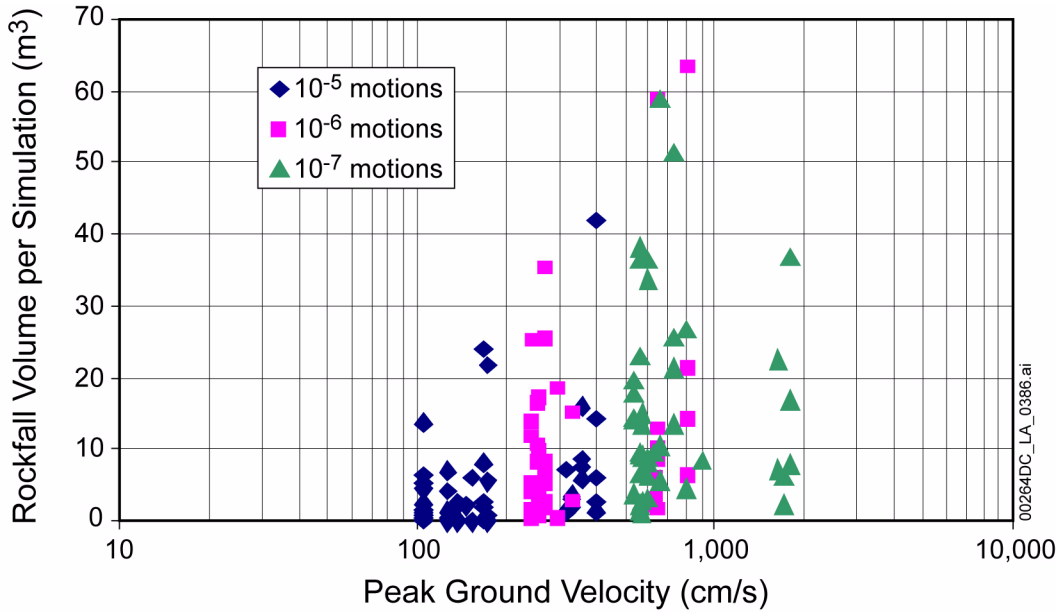

Figure 2.3.4-39. Summary of Rockfall Volume as a Function of Peak Ground Velocity for Nonlithophysal Rock, all Postclosure Hazard Levels

NOTE: The length of drift per simulation is 21.74 m (SNL 2007c, Section 6.7.2). The postclosure hazard levels are unbounded, so the corresponding PGV levels are 1.05 m/s, 2.44 m/s, and 5.35 m/s for the 10^{-5}, 10^{-6}, and 10^{-7} per year exceedance frequencies, respectively. The maximum bounded PGV is 4.07 m/s. The effective drift length that can experience rockfall in the 3DEC model is 21.74 meters (SNL 2007c, Section 6.7.2).

Source: BSC 2004a, Figure 6-83.

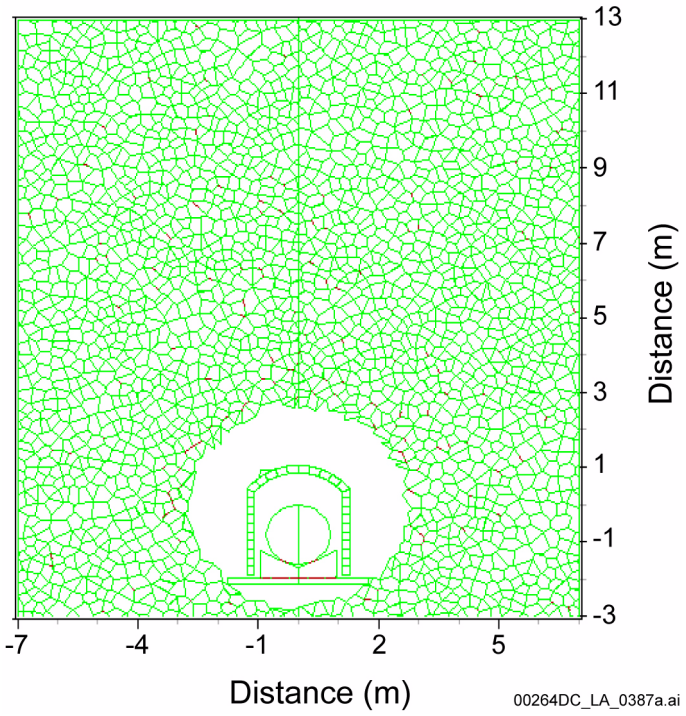

Figure 2.3.4-40. Example of UDEC Discontinuum Model for Lithophysal Rock Showing Emplacement Drift, Drip Shield, Invert, Waste Package, and Pallet

NOTE: Coordinates centered at tunnel midpoint. Rock is a bonded block assemblage calibrated to replicate lithophysal rock mechanical properties.

Source: BSC 2004a, Figure 6-116 (adapted using actual drip shield geometry).

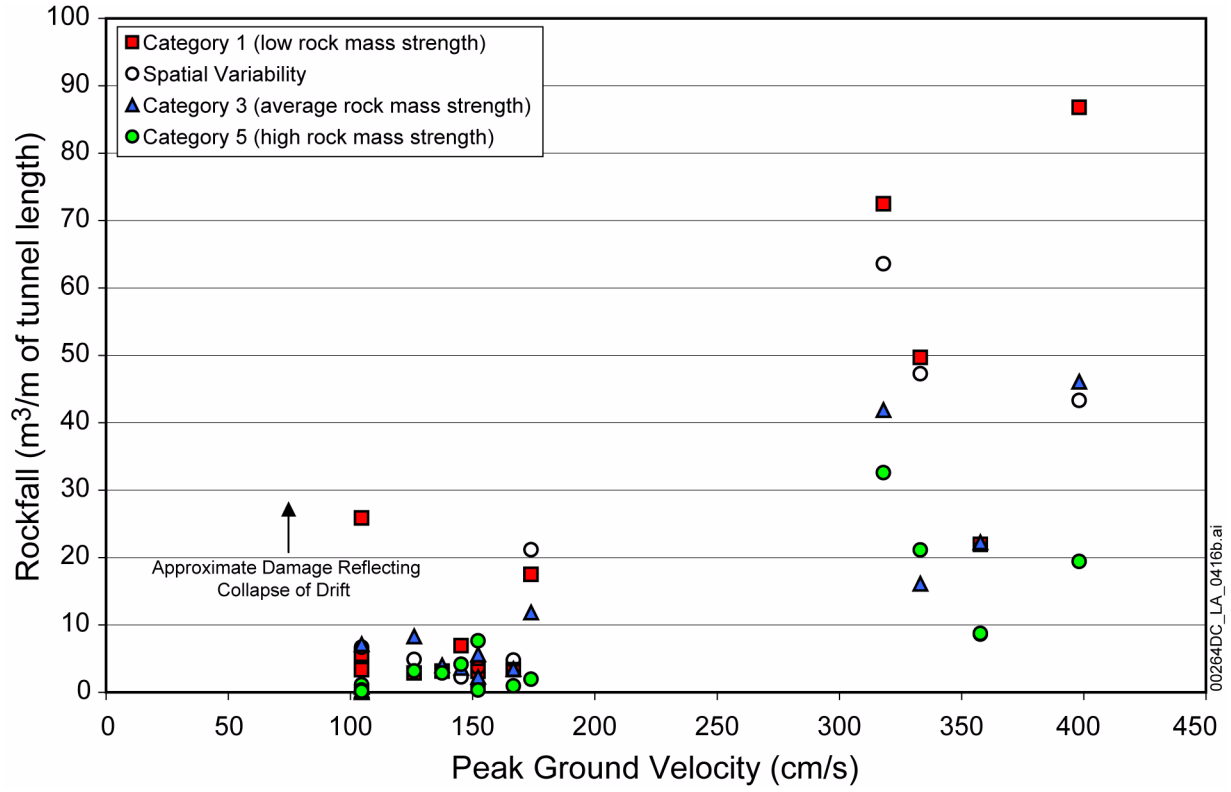

Figure 2.3.4-41. Estimated Lithophysal Rock Damage Level for All 10^{-5} Ground Motion Time Histories, Expressed as m^3/m of Emplacement Drift Length for Rock Strength Categories 1, 3, and 5

NOTE: The maximum value of the unbounded PGV for all three components of a given time history is plotted on the horizontal axis. An approximate linear upper bound to the damage level is evident. Damage level corresponding to collapse of drift is represented as a uniform distribution from 30 m^3/m to 120 m^3/m in TSPA, although the single value of 20 m^3/m was assumed in *Drift Degradation Analysis* (BSC 2004a). Open circles are results for simulations in which rock mass has spatially variable lithophysal porosity and, thus, spatially variable strength.

Source: BSC 2004a, Figure 6-128.

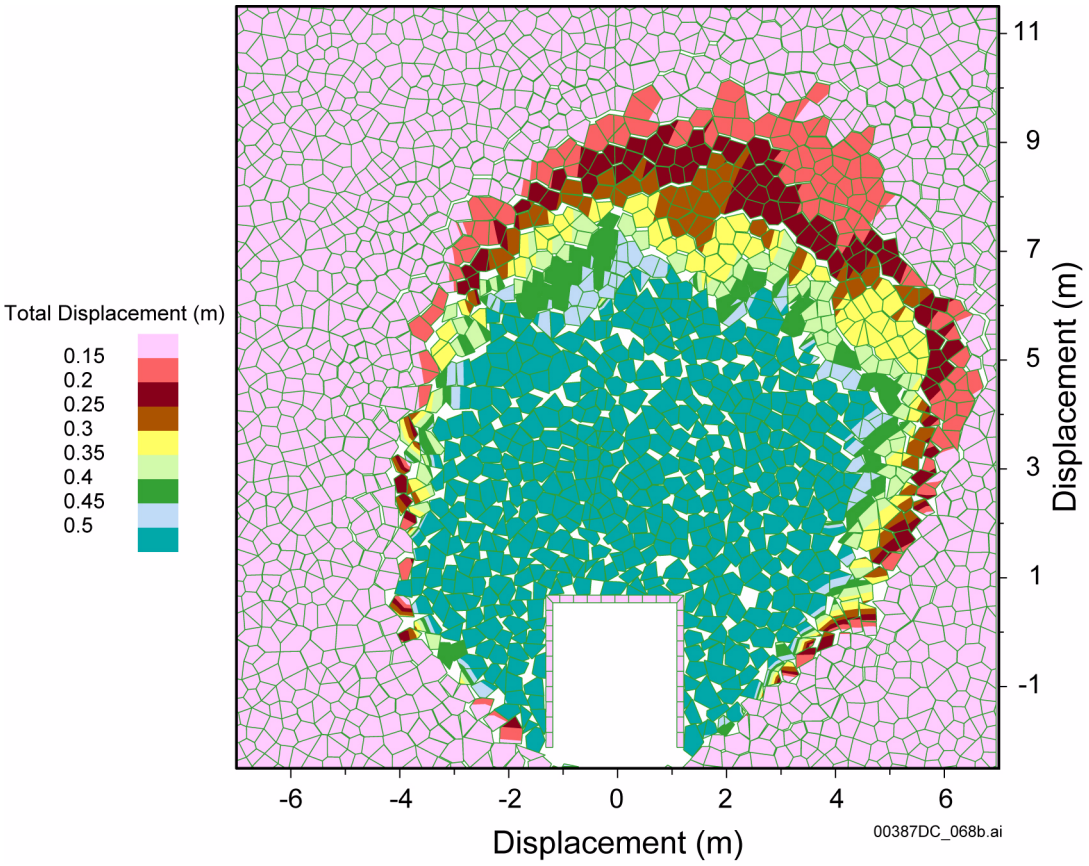

Figure 2.3.4-42. Typical Geometry of the Emplacement Drift in Lithophysal Rock after Simulations for Postclosure Ground Motions with Annual Exceedance Probability of 10^{-6}

NOTE: Rectangular drip shield is shown in tunnel. Ground support will degrade and eventually fail during the postclosure time period, and has not been considered in the rockfall models. Ground motions with an annual exceedance probability of 10^{-6} cause complete collapse of the emplacement drifts irrespective of the rock mass strength category or the particular ground motion time history. Blocks are colored by magnitude of displacement to show extent of collapsed zone. Ultimate drift profile is elliptic in shape with major axis 1 to 2 diameters of the original drift dimension.

Source: BSC 2004a, Figure 6-132(e).

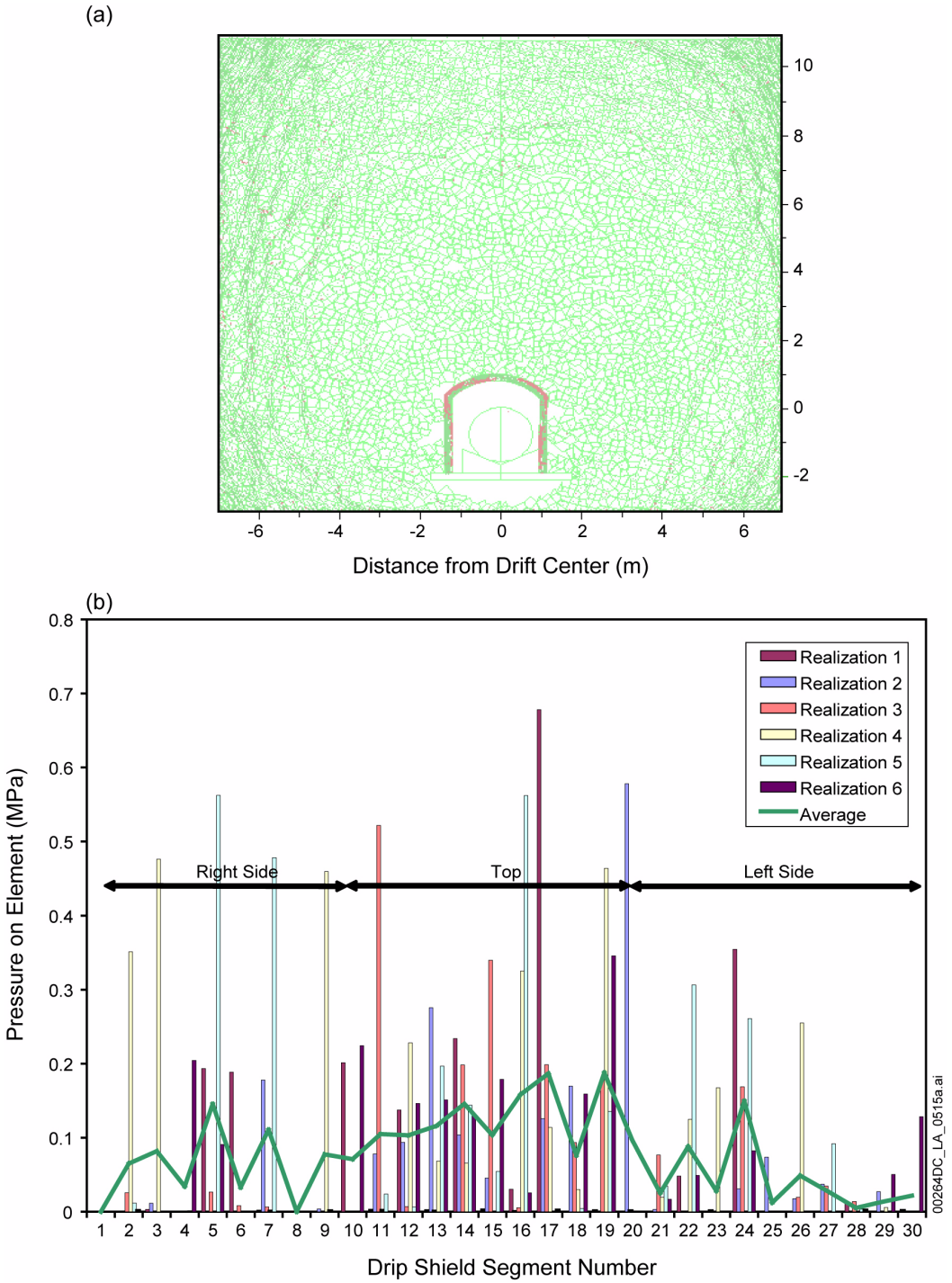

Figure 2.3.4-43. Estimate of Drip Shield Static Load for a Completely Collapsed Drift: (a) Rubble-Filled Drift and (b) Average Pressure on Drip Shield Segments for Six Realizations of Rock Block Structure as well as Average Pressure from All Six Realizations

NOTE: Average pressure on each segment is shown for all six realizations. Segment numbering starts at 1 at right footing and continues counterclockwise to the left footing. Those elements on the right, top, and left sides of the drip shield are shown.

Source: BSC 2004a, Figures 6-172 and 6-174.

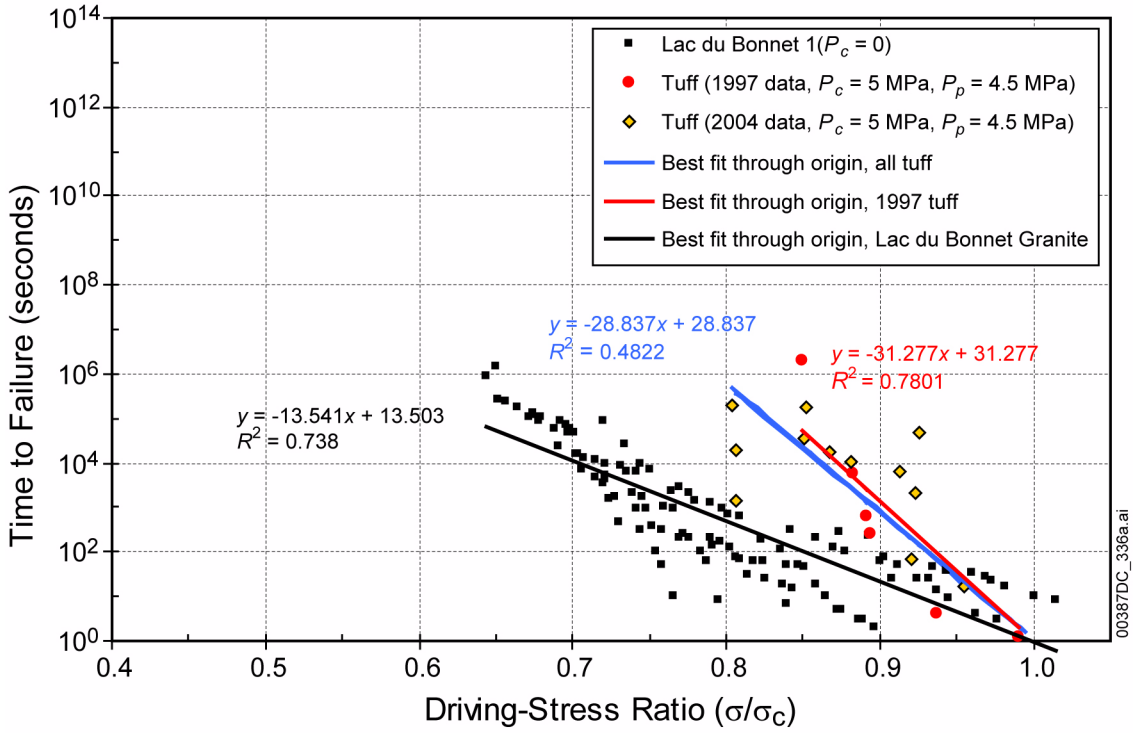

Figure 2.3.4-44. Static-Fatigue Data for Unconfined and Triaxial Compression of Heated, Saturated Welded Tuff and Lac du Bonnet Granite

NOTE: Tests of Lac du Bonnet granite were conducted at 25°C. The driving stress ratio is defined as the ratio of applied constant test stress to the estimated unconfined compressive strength. 1997 tuff tests were conducted at 150°C, and 2004 tests were conducted at 125°C. Linear fits to 1997 Lac du Bonnet only and 1997 and 2004 tuff tests are shown. Samples that did not fail are also shown but not used in developing linear fits to data. P_c is the test confining pressure, and *Pp* is the pore-water pressure.

Source: BSC 2004a, Figure 6-155.

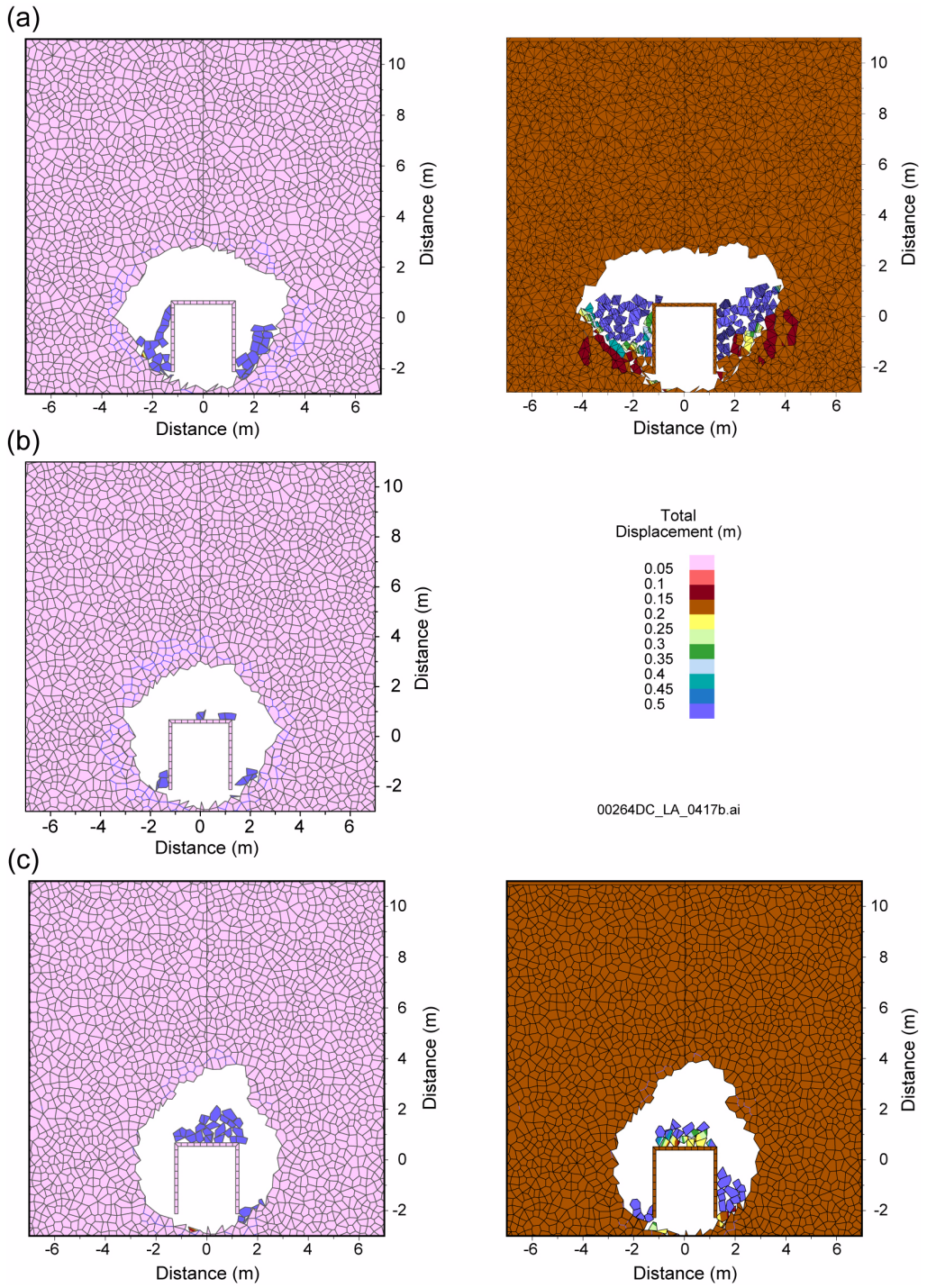

Figure 2.3.4-45. Predicted Time-Dependent Drift Degradation at 10,000 Years for Lithophysal Rock Strength Categories 2 (a), 3 (b), and 5 (c)

NOTE: Blocks colored by displacement magnitude to show extent of detached material. Fracture-damaged zone in plots in left column extends approximately 1 to 2 m into tunnel walls. Left column is from nominal scenario of in situ and thermal stressing only; right hand column is for left column cases after application of shaking with a 0.384 m/s PGV level ground motion.

Source: BSC 2004a, Appendix S, Figures S-43, S-47, and S-48.

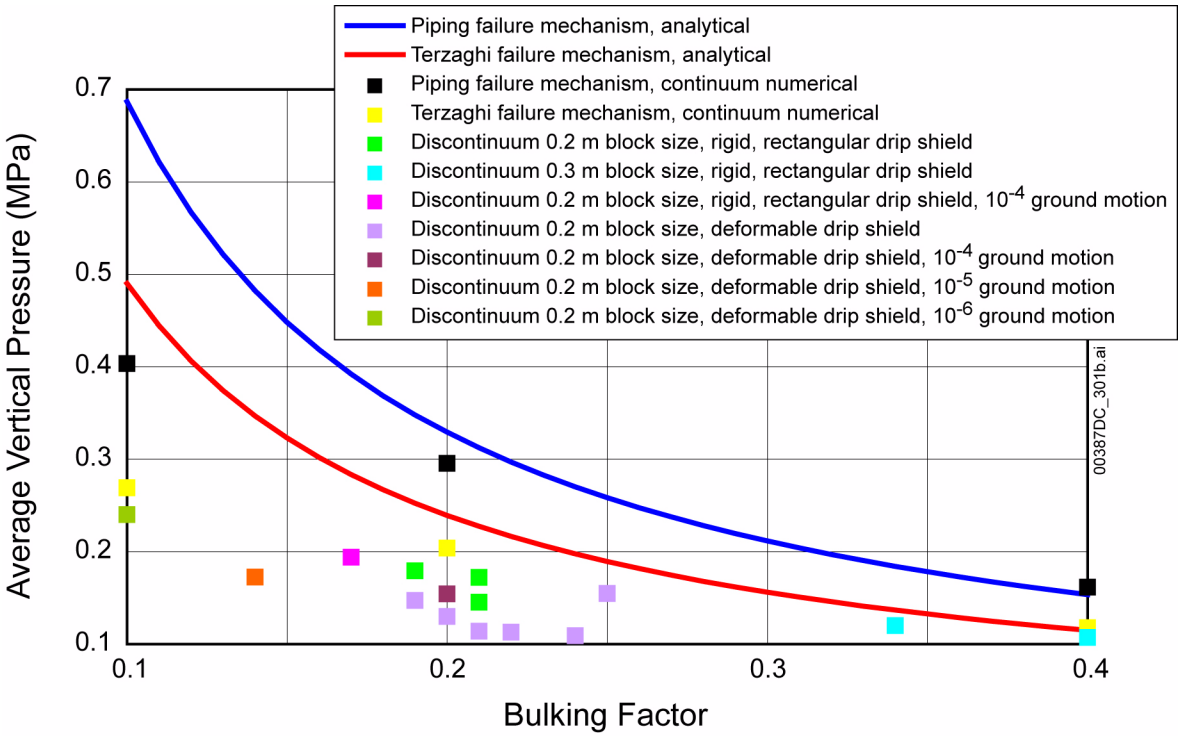

Figure 2.3.4-46. Summary of Average Vertical Pressure Exerted on the Drip Shield as a Function of Bulking Factor Using Discontinuum Modeling Approach versus Several Alternative Analytical Approaches

NOTE: Solid lines show the analytical methods. Symbols are numerical solutions. Various discontinuum realization runs for different assumed block size show range of bulking factors. Effect of rigid versus deformable drip shield is shown. Impact of postcollapse shaking on compaction of rubble and rubble loading is shown.

Source: BSC 2004a, Figure 6-179.

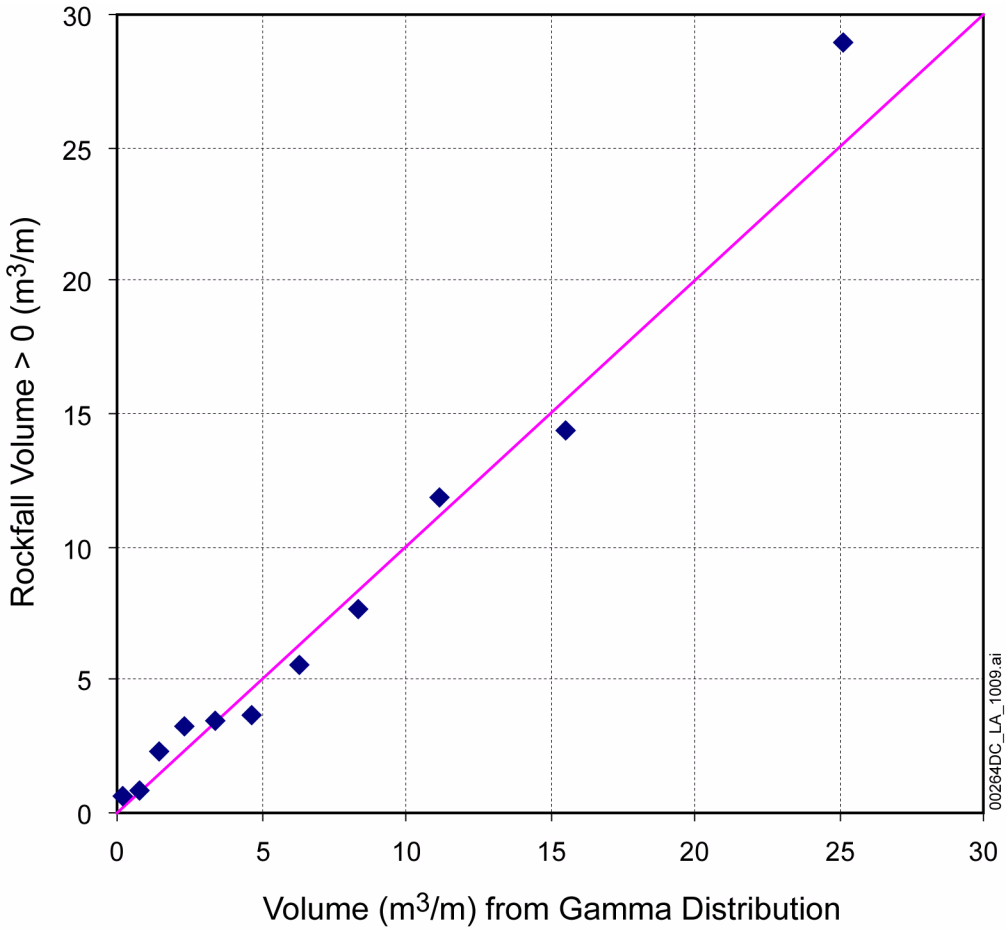

Figure 2.3.4-47. Q-Q Plot for Conditional Lithophysal Rock Volume Versus a Gamma Distribution at the 1.05 m/s PGV Level

NOTE: Rockfall Volume > 0 is the conditional lithophysal rock volume that caves into the drift.

Source: SNL 2007c, Figure 6-54.

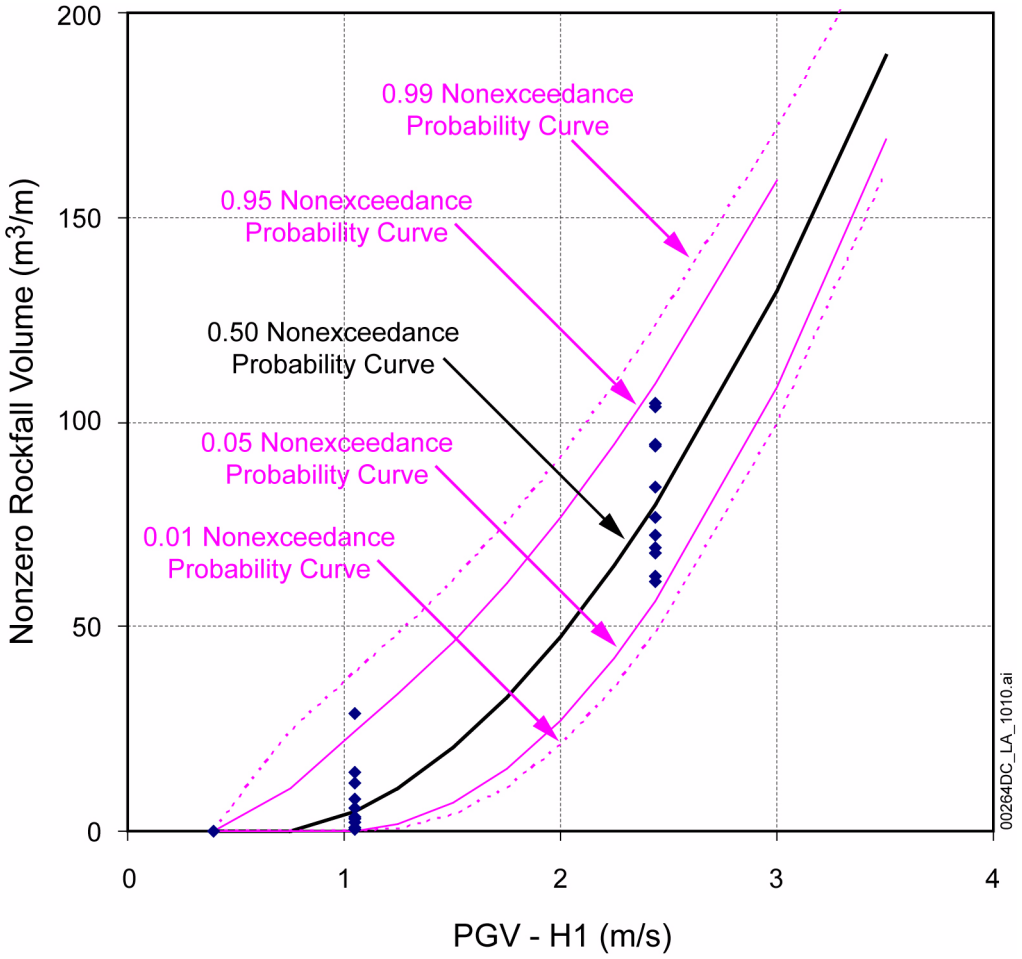

Figure 2.3.4-48. Comparison of Percentiles on the Gamma Distributions for Conditional Lithophysal Rock Volumes

Source: SNL 2007c, Figure 6-57.

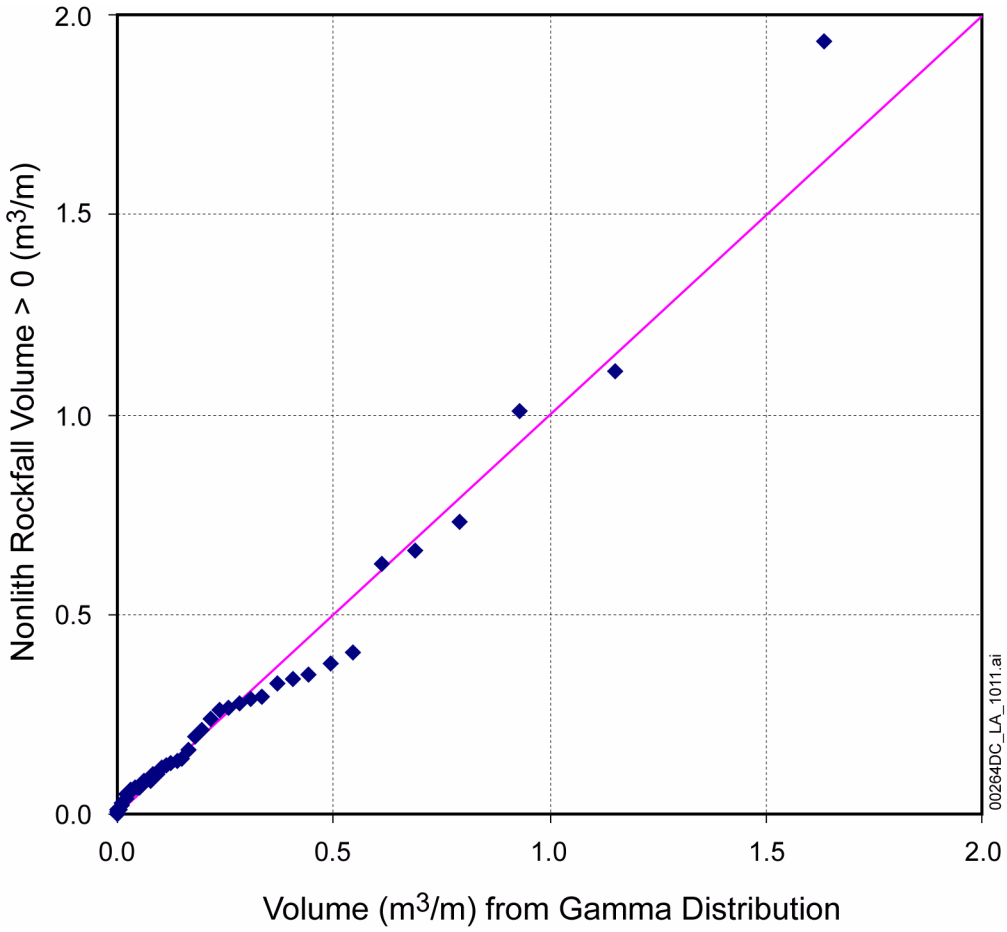

Figure 2.3.4-49. Q-Q Plot for Conditional Nonlithophysal Rock Volume Versus a Gamma Distribution at the 1.05 m/s PGV Level

NOTE: Rockfall Volume > 0 is the conditional nonlithophysal rock volume that caves into the drift.

Source: SNL 2007c, Figure 6-59.

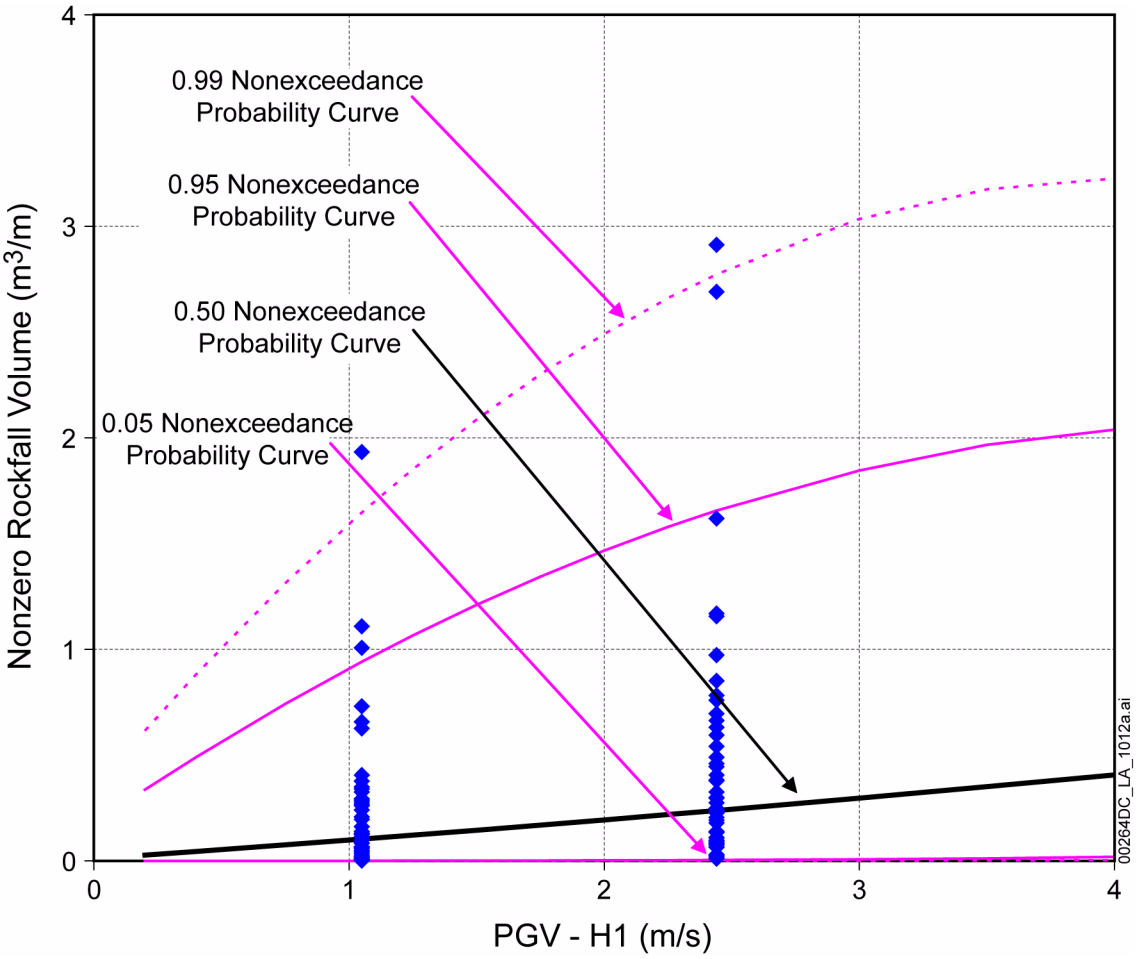

Figure 2.3.4-50. Comparison of Percentiles on the Gamma Distributions for Conditional Nonlithophysal Rock Volumes

Source: SNL 2007c, Figure 6-63.

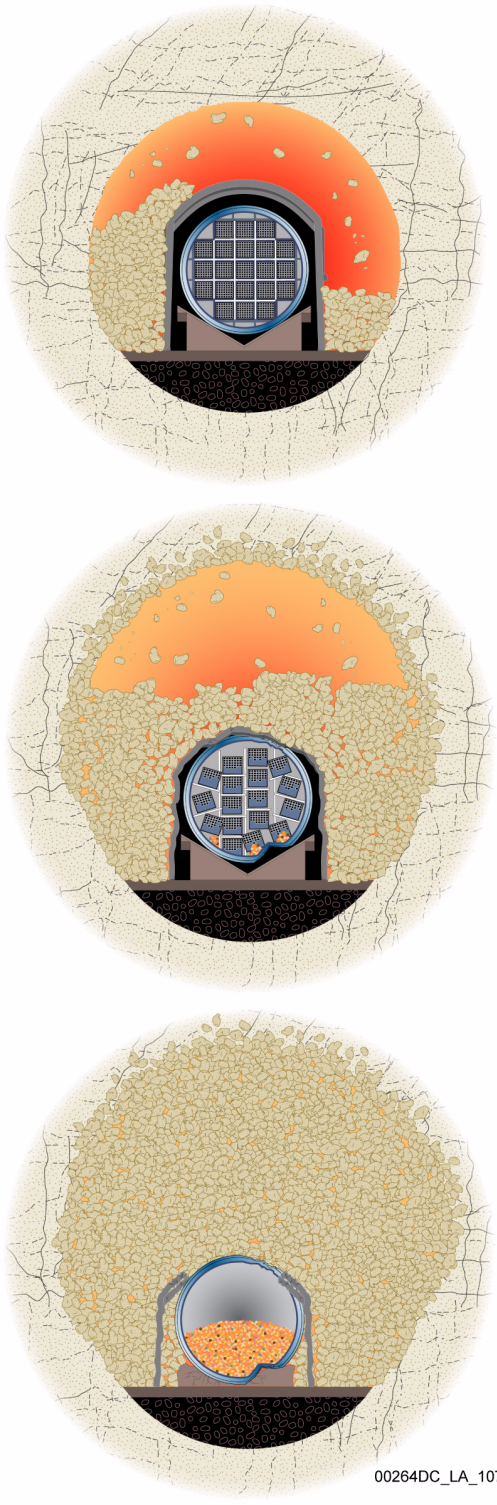

Figure 2.3.4-51. Long-Term Evolution of the Engineered Barrier System (EBS)

NOTE: Three general degradation states of the EBS are envisioned: State 1-Intact Drip Shield, State 2-Drip Shield Failure by Framework Buckling, and State 3-Drip Shield Failure by Plate Rupture.

Source: Modified from SNL 2007c, Figure 6-4.

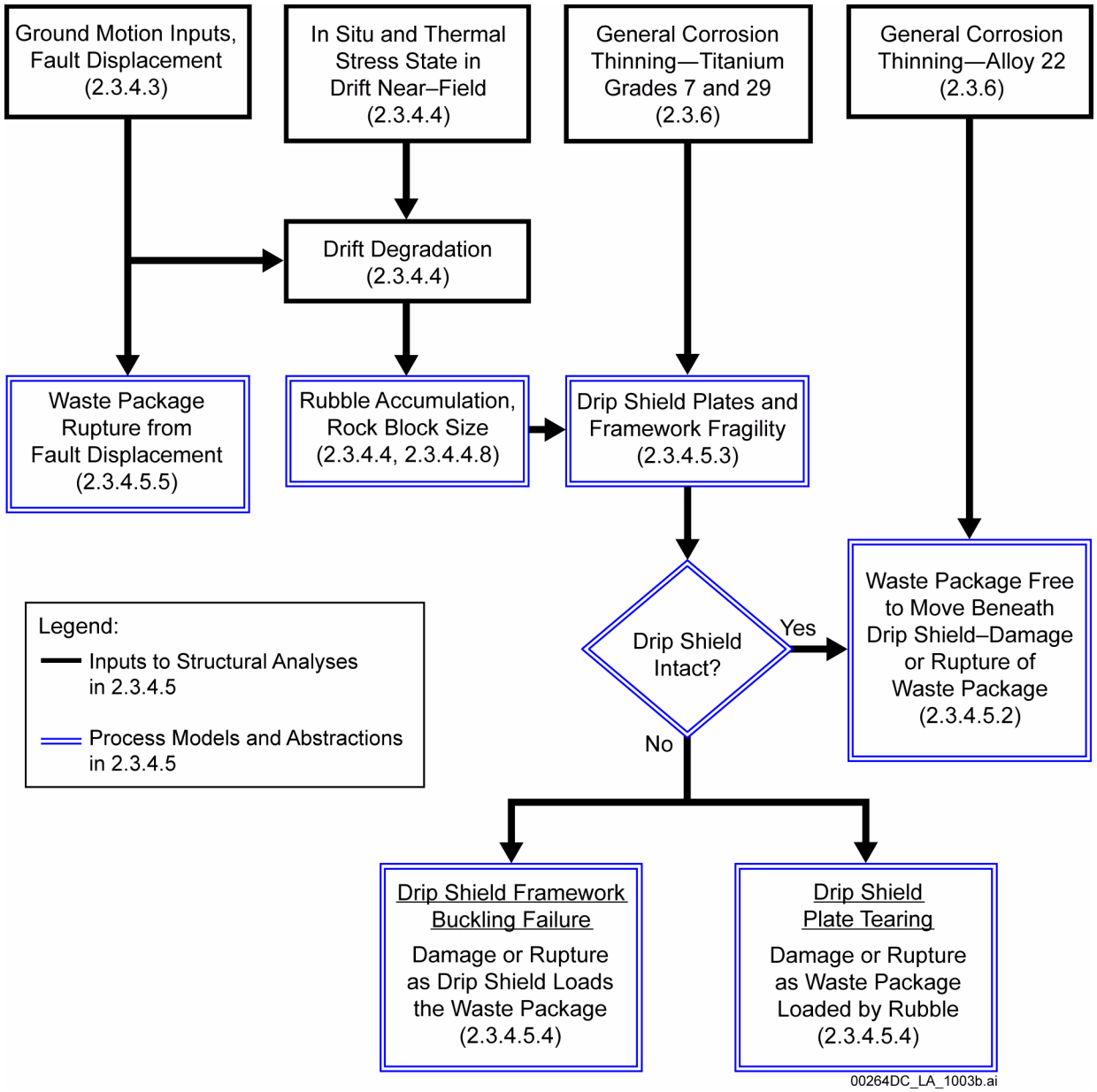

Figure 2.3.4-52. Flow Chart Showing Interrelationship of Process Models Described in Section 2.3.4

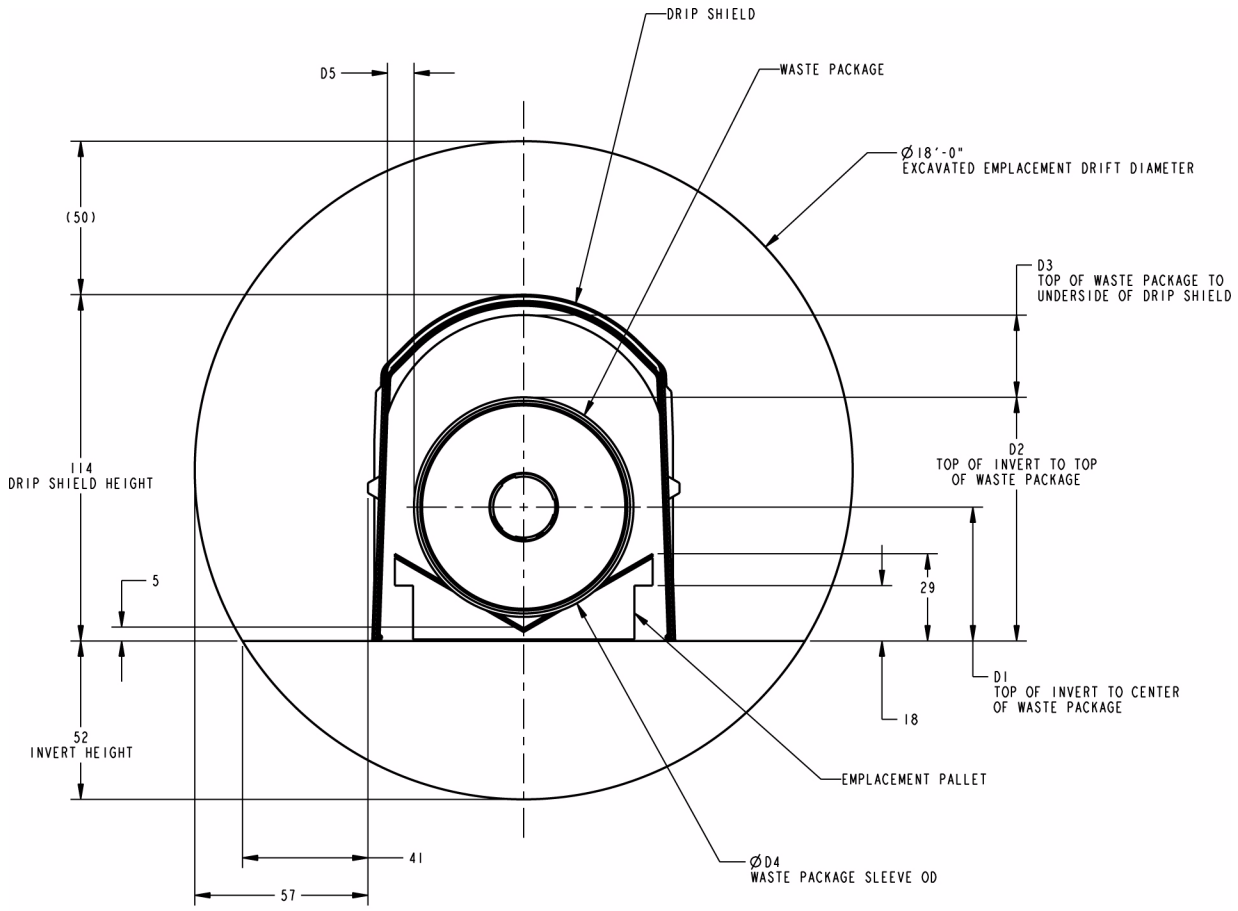

WASTE PACKAGE TYPE	D1	D2	D3	D4	D5
2-MCO/2-DHLW	44	80	27	72	9
NAVAL SHORT/LONG	47	86	21	77	6
TAD	47	86	21	77	6
5-DHLW/DOE SNF SHORT/LONG	51	92	14	84	3

00264DC_LA_1024a.ai

Figure 2.3.4-53. Emplacement Drift Geometry

Source: SNL 2007c, Figure 6-107.